学位論文

Phase relations of Bi- and Bi(Pb)-based superconductors

(ビスマス及びビスマス鉛系超伝導体の相関係)

Doctor of Science

The University of Tokyo, December, 1995

Takuya Suzuki

理学博士(東京大学)　鈴木　拓

東京大学大学院理学系研究科　物理学専攻

Phase relations of Bi- and Bi(Pb)-based superconductors

Doctor of Science

Takuya SUZUKI

The University of Tokyo
1995

Abstract

An high temperature X-ray powder diffraction apparatus combined with an optical microscope has been developed for the first time. The apparatus also has been applied to investigate the phase relations of the Bi- and Bi(Pb)-based superconductors. In this study, pseudo-binary phase diagrams in the Bi_2SrO_4-$SrCuO_2$, $Bi_2Sr_2CuO_6$-$CaCuO_2$ and $(Bi_{0.8}Pb_{0.2})_2Sr_2CuO_6$-$CaCuO_2$ systems are clarified. In addition, the effects of Ca and Pb substitution on the phase diagrams are also clarified and discussed.

The characteristics of the apparatus are as follows, (1) The highest temperature of the samples can be set at 1100 °C and the temperature can be controlled between 1 to 20°C/min by a computer. (2) The sample chamber can be evacuated or filled with air, oxygen, or inert gas. (3) The sample can be set in a horizontal position and rotated around the vertical axis to measure the specimen in a complete or partial melting state. (4) The total counting time of scattered X-rays in the allowed diffraction angle $\Delta(2\theta) \leq 40°$ is less than 1 min. (5) Magnification of the optical system is about 100 times on the TV monitor. (6) The sample can be kept at the right position during the measurement by the microscope focus adjustments. It is found that the developed apparatus can be employed to investigate a phase relation, especially at high temperatures, crystal growth and kinetics of phase transition.

The pseudo-binary phase diagrams in the Bi_2SrO_4-$SrCuO_2$ system is clarified for the first time. The coexisting states of starting solid phase and

liquid are found to exist widely between 10-60°C. This phenomenon is thought to be due to re-crystallization. The incongruent melting point becomes higher with increasing $SrCuO_2$ concentration. In the $Bi_2Sr_2CuO_6$-$CaCuO_2$ system, the liquidus line with high positive in clination is drawn. The pseudo-liquid or partial melting state which is made of a coexistence in staring solid and liquid is also found to exist in this system. The other effects of the Ca substitution are summarized as follows, (1) The substitution changes the way of the change in the incongruent melting temperature of the stoichiometric oxides when their compositions are altered. (2) The substitution results in the instability of the $Bi_2Sr_2CaCu_2O_8$ crystal structure. (3) The substitution leads to better crystallinity in and around grain boundaries in the powder with the $Bi_2Sr_2CaCu_2O_8$ crystal structure. The pseudo-binary phase diagrams of $(Bi_{0.8}Pb_{0.2})_2Sr_2CuO_6$-$CaCuO_2$ system is found to be similar to the $Bi_2Sr_2CuO_6$-$CaCuO_2$ system. The incongruent melting point of $(Bi_{0.8}Pb_{0.2})_2Sr_2Ca_2Cu_3O_{10}$ is the lowest in the stoichiometric oxides. The other effects of the Pb substitution are as follows, (1) The incongruent melting point of Bi(Pb)-Sr-Ca based cuprates are 6~10°C lower than those of Bi-Sr-Ca based cuprate. (2) The amount of liquid above the incongruent melting points of Bi(Pb)-based cuprates is larger than that of Bi-based cuprates. (3) The amorphous phase exists in the temperature range of about 50°C above the incongruent melting point of $(Bi_{0.8}Pb_{0.2})_2Sr_2Ca_2Cu_3O_{10}$ and $(Bi_{0.8}Pb_{0.2})_2Sr_2Ca_{2.5}Cu_{2.5}O_x$. Due to the effect (2), these oxides are thought to be able to synthesize easily because so-called liquid phase sintering is available. In addition, it should be noted that the Pb

substitution leads to the possibility for growing high quality large single crystals of $(Bi_{0.8}Pb_{0.2})_2Sr_2CaCu_2O_8$ and $(Bi_{0.8}Pb_{0.2})_2Sr_2Ca_2Cu_3O_{10}$ using the peritectic reaction in a slow cooling method from a solid and liquid coexisting state, because a large amount of the liquid exists above the peritectic temperature.

Contents

Chapter 1. General introduction

Since phase relations, usually phase diagrams, on multi-component materials are generally very complex, a few studies on them have been reported. They are classified into two large groups. One is on the earth science and the other is on the material science. In the earth science, the phase relation under not only high-temperature but also high pressure are important to investigate the origin of the earth [1,2]. The phase diagrams only in the specified system concerned with the earth have been clarified [3]. In the material science, the phase relations are basic data on growing single crystal, on synthesizing non-equilibrium materials, and on controlling mechanical and physical properties for industrial usage[4].

Most of the multi-components materials investigated on the phase diagram are oxides, especially magnetic and electric materials. High-temperature superconductive oxides are one of the typical materials and have been well investigated [5], such as $1/6YBa_2Cu_3O_{7-\gamma}$- $1/10Ba_3Cu_7O_{10}$ system in Figure 1.1 [6]. Identification of a quenched sample is the most typical and conventional method to investigate the phase relation. This is often called "the quenching method". This method is easy to apply and has produced numbers of phase diagrams. However, it has some problems to decide the phase relations, and the most fatal problem occurs in the easewhere a liquid phase coexists with a solid. When a sample of concentration X at temperature t_1 in Figure 1.2 is

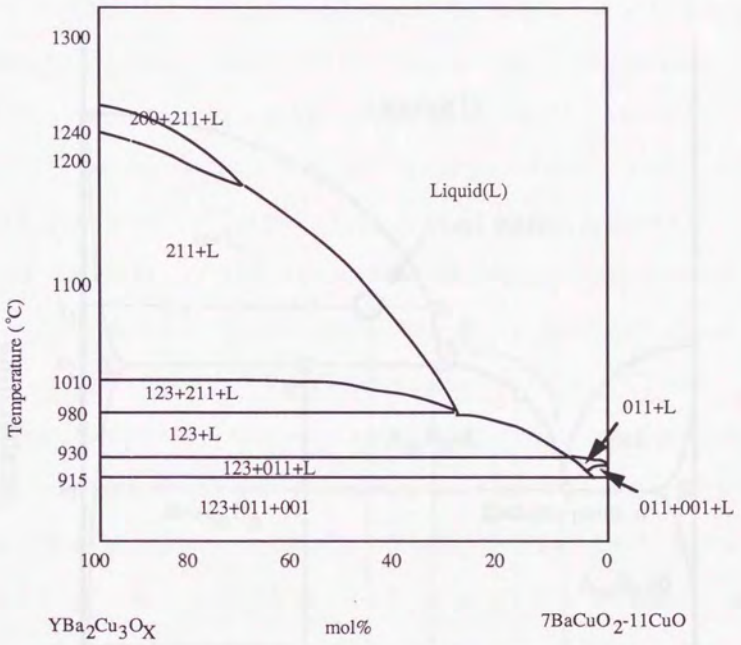

Fig. 1.1 A binary section of the ternary phase diagram.
The phases are labeled as follows,
123: $YBa_2Cu_3O_{7-x}$ 011: $BaCuO_2$
211: Y_2BaCuO_5 200: Y_2O_3
001: CuO

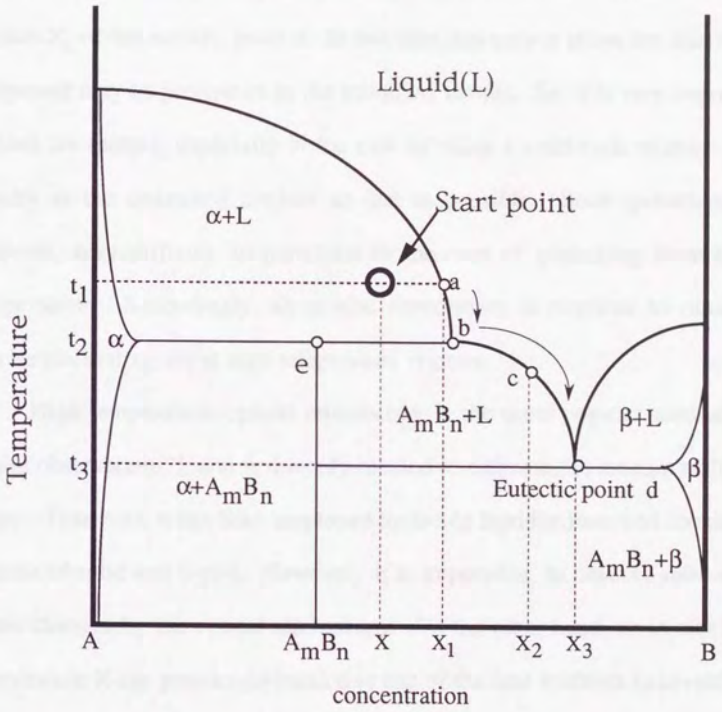

Figure 1.2 Phase diagram in the A-B system.
α and β mean solid solutions. A_mB_n means compound.

quenched very rapidly, one can identify only α phase in the quenched sample. However, if the sample is cooled not so rapidly, the concentration of the liquid phase changes from X_1 to X_2 along the liquidus line a $\rightarrow$ b $\rightarrow$ c, and it finally reaches X_3 of the eutectic point d. In this case, not only α phase but also A_mB_n compound may be precipitate in the solidified sample. So, it is very important to cool the sample, especially in the case of using a solid-melt mixture very rapidly in the quenched method as fast as possible. Such quenching is, however, very difficult, in particular in the case of quenching from high-temperature. Accordingly, an in-situ observation is required to obtain a precise phase diagram at high temperature regions.

High-temperature optical microscopy is the most popular method for in-situ observation[7], and is the only method to estimate the amount of liquid phase. Therefore, it has been employed to decide liquidus lines and coexisting regions of solid and liquid. However, it is impossible to observe solid-solid phase changes by the optical microscopy. On the other hand, an in-situ high temperature X-ray powder diffraction is one of the best methods to investigate the phase changes of solids. This method can detect directly and sensitively the phase changes at the atomic scale. However, X-ray diffraction method is not good for estimating the amount of liquid because no diffraction without hallows occurs. Accordingly, an in-situ observation by the combination of optical microscopy and X-ray diffraction is required to decide the precise phase relations at high temperatures. In particular, such an observation is

essential in the case of investigating the multi-component system where the phase diagram is very complicated and has a very narrow temperature range and/or a narrow composition region, as for the example shown in Figure 1.1. Besides, if this in-situ technique is established, it might be powerful for the application to all of studies concerned with phase transition phenomena of substances.

In the present study, an X-ray powder diffraction apparatus combined with an optical microscope has been developed for the first time. The apparatus has been applied to investigate the phase relations of the Bi-based and Pb-based cuprate superconductors. They are typical multi-component materials composed of more than four kinds of elements. For example, Pb-based cuprate superconductors are in the Bi-Pb-Sr-Ca-Cu-O systems. In addition, these phase relations and phase diagrams of the systems are very complicated and have not been established yet, even though they are significantly important materials because of the high utility for low temperature industries, such as high critical temperature (Tc) more than 100K, high critical magnetic field (Hc), low toxicity and economical starting materials. Their phase relations are essential not only for synthesizing the Bi-based superconductive materials but also growing their single crystals, and are also important to investigate the formation and kinetics of the series of oxides. Therefore, the establishment of the phase diagrams is a key for investigating the high-temperature superconductivity as well as for producing superconductive wires, devices and magnets and so on.

The first purpose of this study is to develope the apparatus for the in-situ high-temperature observation combining both optical microscope and X-ray powder diffraction. The second purpose is to investigate the phase relations in the Bi-Sr-Cu-O, Bi-Sr-Ca-Cu-O and Bi-Pb-Sr-Ca-Cu-O systems, especially the effects of the substitutions of Ca for Pb. In Chapter 2, the development of the apparatus and the establishment of the best conditions for the operation are described. In Chapter 3, the pseudo-binary phase diagrams in the Bi_2SrO_4-$SrCuO_2$, $Bi_2Sr_2CuO_6$-$CaCuO_2$ and $(Bi_{0.8}Pb_{0.2})_2Sr_2CuO_6$-$CaCuO_2$ systems are clarified using the apparatus. Besides, the formation mechanism of a series of oxides is discussed. The scientific contributions by this study are summarized in Chapter 4.

References

[1] Y. Matsui and S. Sakano : Earth chemistry of rocks and minerals, (*Iwanami*, 1992,Tokyo)

[2]A. Tsuzuki : Metamorphic rocks and zones, (*Iwanami*, 1965, Tokyo)

[3] S. Akimoto and J. Mizutani : Earth material science 1 (*Iwanami,* 1978,Tokyo)

[4]R. M. German : Liquid phase sintering (*Plenum Publishing Co.* 1985,New York)

[5] John D. Whitler and Robert S. Roth : Phase diagrams for high Tc superconductors (*The American Ceramic Society*, 1991, New York)

[6] K. Dembinski, M. Gervais, P. Odier and J. P. Coutues, *J. Less-Common Metals* **164/165** (1990) 177

[7] For example, :The handbook of crystal growth,(*Kyoritsu Pub. Co.* 1995, Tokyo)

Chapter 2.

Development of apparatus for in-situ high-temperature optical microscope and X-ray powder diffraction observation

2.1 Introduction

X-ray diffraction method is commonly used for the phase identification for the studies on phase stability relations and phase transition. Most of the apparatus for high-temperature examination are made of a horizontal type goniometer or a four circle auto diffractometer with a furnace. They are suitable for measurements of a change in solid but not for investigating a change in melt at high temperatures. A vertical type goniometer combined with a furnace is recently popular [1]. In addition, an X-ray diffraction pattern with high signal-noise ratio requires a long counting time over 20 minutes, even though a high time-resolution below a few minutes is necessary for studying in kinetics of phase transition. Accordingly, time-resolved X-ray detectors such as Imaging Plate (IP), Position Sensitive Detector(PSD), Solid State Detector (SSD) and a Position Sensitive Proportional Counter (PSPC) have been employed instead of a conventional scintillation counter for such studies. IP is a kind of two-dimensional detector using photo-stimulated luminescence. However, IP has no capability for a high time-resolution because of the need of accumulation and data reading time. In addition, the measuring energy range are relativity high between 15 and 25 keV which is realized in a synchrotron orbital radiation (SOR) [2]. SSD has a high sensitivity and energy resolution. However, X-ray powder diffraction (XPD)

measurements using SSD require a continuous X-rays from such as SOR. Besides, SSD has some annoying corrections by removing escape peaks, by separating multiple peak profiles and by intensity evenness at each incident X-ray energy [3-5]. PSD uses a thin metal plate as an anode at self-extination streamer mode. A delay line system is used to detect the position of diffracted beams. It has been often used for high pressure and high-temperature XPD experiments[6], but is very complicated and expensive. PSPC is more conventional and is used popularly instead of the usual proportional counter. It is composed of uses a metal wire as an anode at an proportional counting area[7,8], and can measure at a wide 2θ area (5-110°) with time less than a few minutes because of a high sensitivity. Oyama et al. developed a time-resolved high-temperature X-ray powder diffraction (HT-XPD) apparatus using a PSPC for in-situ and rapid measurements [9]. They measured $YBa_2Cu_3O_x$ (Y-123) crystal growth rate at a slow cooling from Y_2BaCuO_x + liquid phases and investigated kinetics of Y-123 and crystal growth mechanism [10]. Quite recently, we measured a crystallization rate of Bi-2201 and a crystal growth rate of Bi-2212 from a glassy state and proposed a crystal growth mechanism of Bi-2212 [11]. As mentioned above, XPD using the time-resolved counter like PSPC is very useful for the investigation of structure changes at atomic scale. However, it is powerless for detecting the presence of a liquid phase in a sample.

An optical microscopy has been well employed for an in-situ observation

of a dynamical change in solid and/or solid and melt. A lot of studies on crystal growth mechanisms [12], concentration measurements of distribution at the solid liquid interface [13], phase relations [14] and crystal habit changes under high pressure[15] have been carried out using the in-situ optical microscope. This method is very suitable for observing a melting behavior and crystal habit changes, but not for detecting changes in a solid phase. Accordingly, the development of the combined apparatus of HT-XPD and optical microscope is actually important. In this chapter, the development of the apparatus is described, the basic frame-work of which has been developed by Oyama et al. [9]

2.2 Total system of apparatus

The high-temperature optical microscope and X-ray powder diffraction system is schematically shown in Figure 2.1. A photograph of the whole view and a magnified feature of the furnace were shown in Figure 2.2. Most of the XPD system is almost the same as that reported by Oyama et al. [9].

The XPD system is composed by a PSPC, a goniometer, an X-ray generator with controller (made by MAC Science Co., MXP-3), a work station (NS/SUN SP1/+) and a multi-channel analyzer (Cannbera, MCA-20). In this study, this system has been partially revised in order to overcome the following problems, (1) a sample exchange requires the furnace to be disjointed, (2) the positional change of the sample stage by heating can not be corrected,

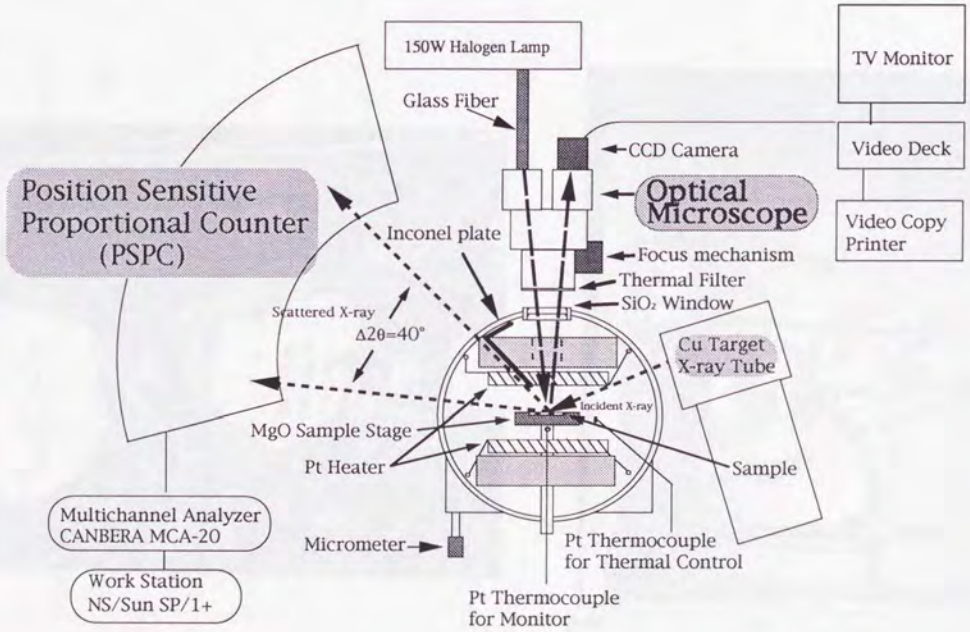

Figure 2.1 Scheme of the apparatus for in-situ high-temperature microscope and X-ray observations.

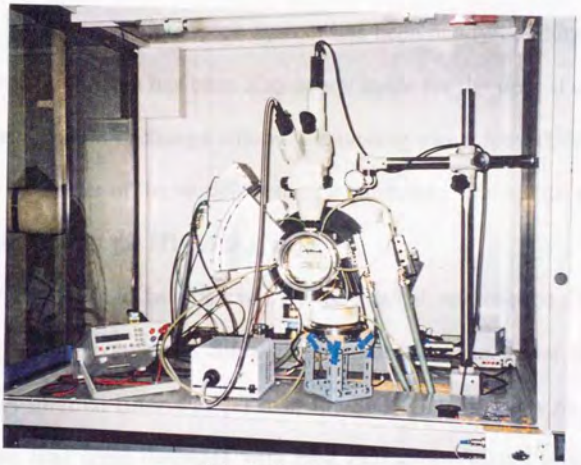

(a)whole view.

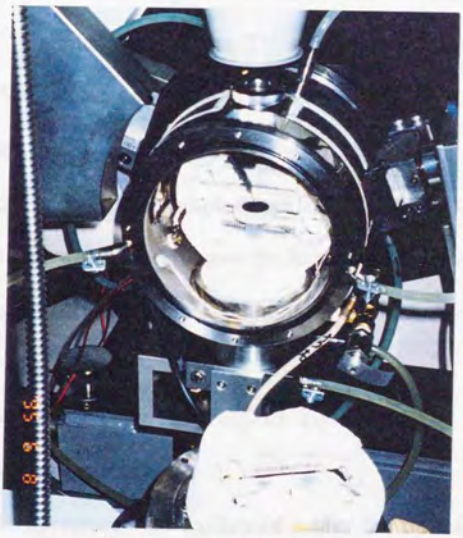

(b) close up of the furnace.

Figure 2.2 Photographs of the apparatus.

and (3) the PSPC can not be operated with the constant sensitivity. In addition, the optical microscope system has been newly combined with the revised one. A furnace has been also newly made for the optical observation and, an easy sample exchange without disjointing was achieved. The furnace was set at the center of the vertical setting goniometer. The optical microscope system was set over the HT-XPD system.

The sample can be observed by the optical microscope (Nikon Co., Ltd., SMZ-2T) through the SiO_2 glass window on the upper side of the furnace. A thermal filter was set over the SiO_2 glass window to protect the microscope lens from damages with heat radiation. Visual images can be filmed by the CCD camera and observed on the TV monitor, where the magnification is about 100x on the TV screen. The images can be also saved by an S-VHS video recording system (Mitsubishi Co., Ltd., HV-P62), and also printed by a video copy processor (Mitsubishi Company, Ltd., CP-15). In order to keep the sample stage at the right focussing position, a furnace micrometer was added below the furnace for adjusting. An Inconel plate was set in the furnace to mask scattered X-ray radiations.

2.3 Establishments of measurement conditions

2.3.1 Sample temperature

Sample temperature was calibrated under the optical microscope by observation of the melting of KCl(Tm=770 °C), NaCl (801 °C), PbO (880 °C) and Ag (961 °C). Figure 2.3 shows the temperature calibration curve,

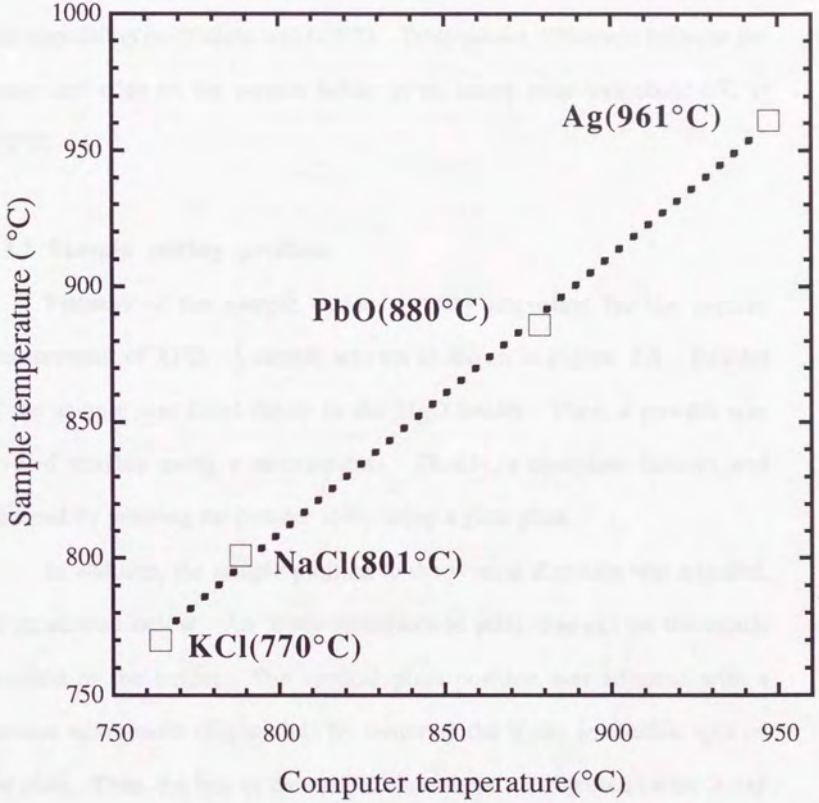

Figure 2.3 Sample temperature calibration curve.

where a linear relation is obtained in the temperature range between 770 and 961°C, as the following equation,

[Sample temperature(°C)]=-8.1+1.0243 × [Computer temperature (°C)]

The correlation coefficient was 0.9992. Temperature difference between the center and edge on the sample holder in an empty state was about 6°C at 850°C.

2.3.2 Sample setting position

Flatness of the sample surface is very important for the precise measurement of XPD. A sample was set as shown in Figure. 2.4. Powder of the sample was filled firstly in the MgO holder. Then, a powder was leveled roughly using a microspatula. Finally, a complete flatness was obtained by pressing the powder softly using a glass plate.

In addition, the sample position in the vertical direction was adjusted, as mentioned below. An X-ray fluorescence plate was put on the center position of the holder. The vertical plate position was adjusted with a furnace micrometer (Figure 2.1) by centering the X-ray irradiation spot on the plate. Then, the lens of the optical microscope was focused on the X-ray fluorescence plate surface.

When the powder sample was calcined and then melted during measurement, the volume decreased, and the position of specimen surface was lowered. Therefore, the sample surface had to be reset at the exact

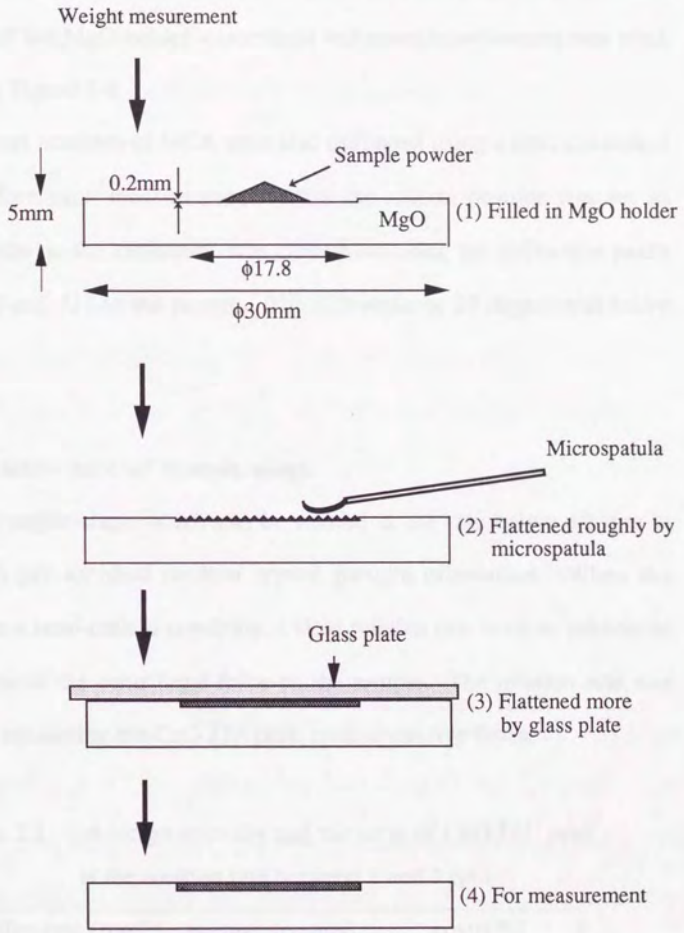

Figure 2.4 Flow chart for setting a sample.

position with the furnace micrometer by adjusting the focus. MgO single crystal is the best material of the holder to avoid a creeping out of the melt. The shape of the MgO holder was critical and some improvement was tried, as shown in Figure 2.4.

Channel numbers of MCA were also calibrated using a silicon standard powder before each measurement. After the silicon powder was set as mentioned above, the calibration was carried out using the diffraction peaks of *111*, *220* and *311* in the pattern. The difference in 2θ degree was below $\pm 0.03°$.

2.3.3 Rotation rate of sample stage

The sample stage which can be rotated at the rate below 12 rpm is provided to get an ideal random crystal particle orientation. When the sample is in a semi-melted condition, a slow rotation rate is more suitable to avoid effects of the centrifugal force on the sample. The rotation rate was selected by measuring the CuO $\bar{7}11$ peak intensity in five times.

Table 2.1 Average intensity and the error of CuO $\bar{7}11$ peak at the rotation rate between 2 and 5 rpm.

Rotation rate (rpm)	average (counts)	error(%)
2	640.5	±20.5
3	644.6	±5.0
4	640.0	±5.2
5	644.7	±2.4

Table 2.1 shows the results at the rotation rate of 2, 3, 4 and 5 rpm. The stable rotation could not be obtained below 2 rpm because of the low limitation in motor torque. Accordingly, the rotation rate was set at 5 rpm due to both of the lowest rate and the most stable rotation.

2.3.4 Operation conditions for PSPC

It is necessary to operate the PSPC in a highly sensitive and stable condition in order to measure fast phase changes. A mixed gas of 90% Ar-10% CH_4 was flowed in the PSPC at a flowing rate of 4 ml/min. The sensitivity and stability of the PSPC are influenced by gas pressure and impurity gases, such as O_2 and H_2O in the counter. A microscale pressure valve with a pressure gauge of 1/1000-atm scale in the minimum scale were used to control the pressure of flowing gas. A gas filter (Osaka Sanso Industry. Co., Ltd. MOC-C-20) was also set in a gas line to remove the impurity gases.

The relation of the gas pressure, applied voltage and counter sensitivities has been investigated. Integrated intensities of the CuO $\bar{1}11$ peak were measured by the PSPC when the gas pressure was between 1.000 and 1.200 atm and the applied voltage was between 2800 and 3300 V. A relationship between the sensitivity and the applied voltage at various gas pressures was shown in Figure 2.5. The PSPC background from a glass plate were checked at various different applied voltages between 2800 to 3300 V. The X-ray diffraction background pattern was distorted above 3150V, and ghost

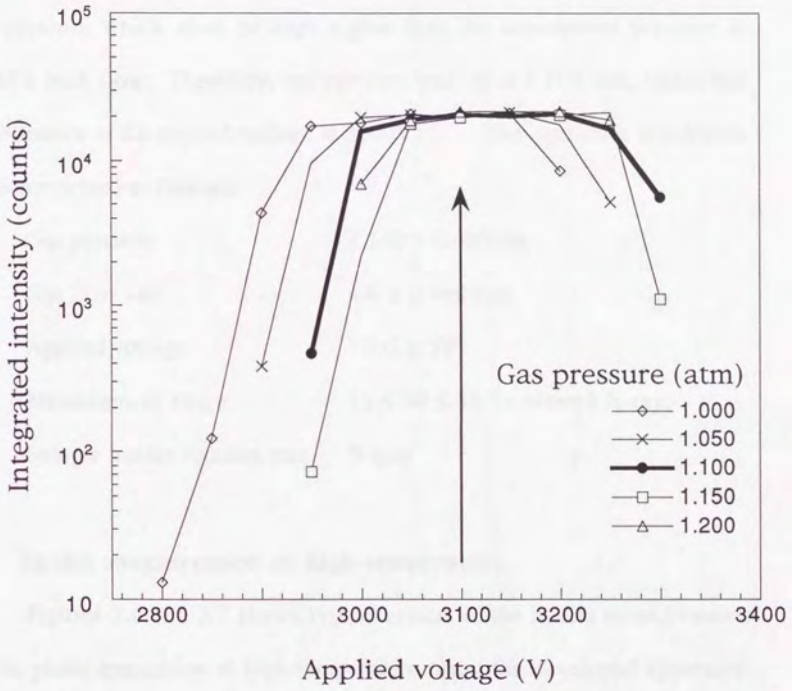

Figure 2.5 Relationship between PSPC sensitivity and applied voltage at various gas pressures.

peaks appeared at around $2\theta = 40°$ above 3200V, although high sensitivity was generally obtained with higher applied voltage. Accordingly, the applied voltage was set at 3100V because of the balance of background noise and high sensitivity. The sensitivity of the counter was influenced with flowing gas pressure which must be kept higher than the atmosphere pressure to avoid a back flow. Therefore, the pressure was set at 1.100 atm, which has no influence to the applied voltage at 3100V. The optimum conditions are summarized as follows:

Gas pressure	1.100 ± 0.005atm
Gas flow rate	4.0 ± 0.1ml/min
Applied voltage	3100 ± 5V
Measurement range	$15 \leq 2\theta \leq 55$ °(scattered X-ray)
Sample holder rotation rate	5 rpm

2.4 In-situ measurement at high-temperature

Figures 2.6 and 2.7 shows typical results of the in-situ measurements of the phase transitions at high-temperature using the developed apparatus. These are XPD patterns and video pictures, showing decomposition and melting at the composition of Bi-2212 [16]. This experiment was carried out on heating run between room temperature and 1000°C at a heating rate of 10°C/min. Figures (a), (b) and (c) correspond to the XPD patterns at room temperature, 910 and 960°C, respectively. At room temperature, the sample was black and identified with Bi-2212 phase from the XPD patterns.

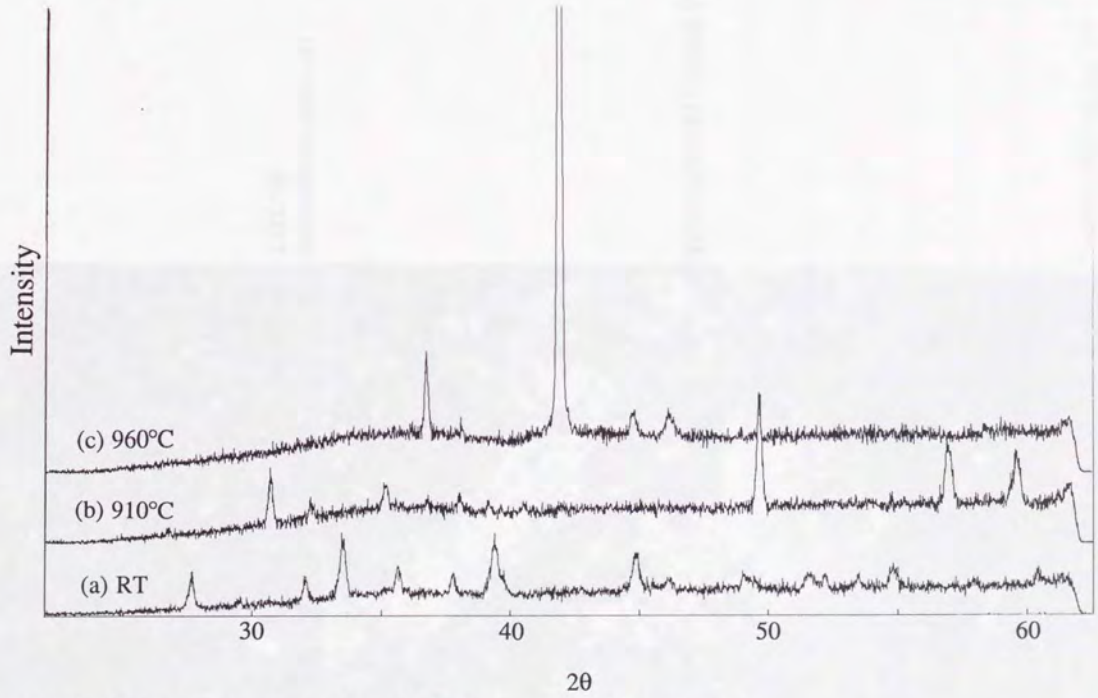

Figure 2.6 Phase changes observed by the XPD pattern (Cu Kα radiation).

(a) at room temperature : Bi-2212, (b) at 910°C : (Sr,Ca)CuO_2+L, (c) at 960°C : (Sr,Ca)O+L.

(c) 950°C : (Sr,Ca)O+L

(b) 920°C : $(Sr,Ca)CuO_2$+L

(a) room temperature : Bi-2212

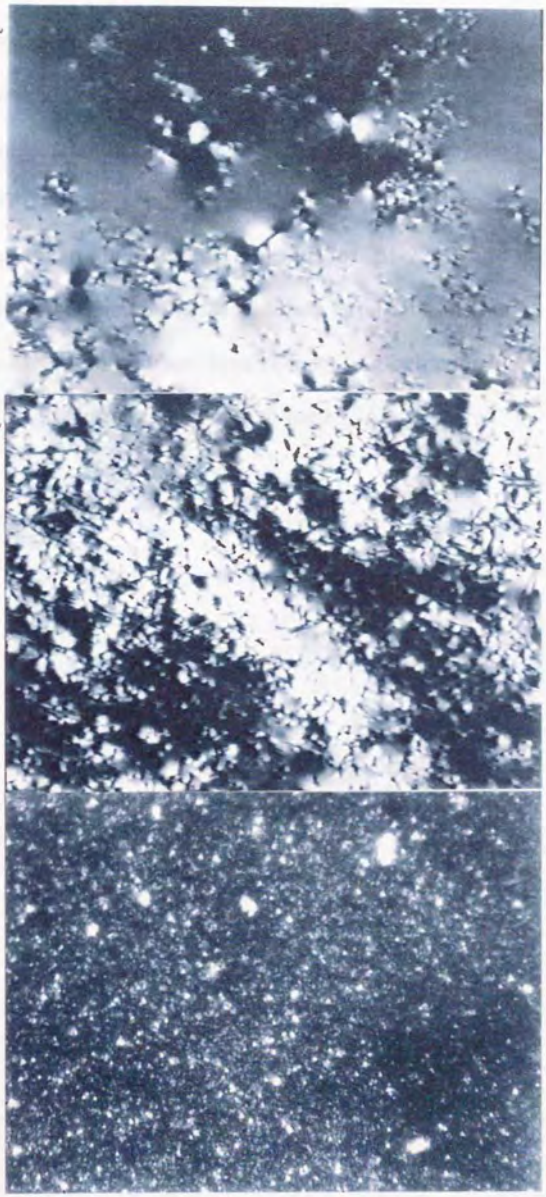

Figure 2.7 Video pictures observed simultaneously with the XPD patterns in Figure 2.6.

At 910°C, needle like crystals in the liquid was observed by the optical microscope. The crystals was identified with (Sr,Ca)CuO_2 from the in-situ XPD results. Besides, a large amount of liquid and small floating crystal chips was observed at 960°C. The small crystals was identified to be (Sr,Ca)O by XPD. These mean incongruent meltings of Bi-2212 and (Sr,Ca)CuO_2 phases. As described above, the developed apparatus in this study makes it possible to observe phase transitions and melting behavior in a semi-quantitative way by the in-situ XPD and optical microscope.

2.5 Summary

The high temperature X-ray powder diffraction apparatus with PSPC combined with the optical microscope has been developed. The operation conditions of the developed apparatus have been optimized. The characteristics of the apparatus are as follows,

(1) The highest temperature of the sample can be set at 1100 °C and the temperature is controlled between 1 to 20°C/min by a computer.

(2) The sample chamber can be evacuated or filled with air, oxygen, or inert gas.

(3) The sample is set in a horizontal position to measure the sample in a molten state and an be rotated around the vertical axis in order to obtain an idealized powder diffraction pattern.

(4) The counting time which is enough for the allowed diffraction angle $\Delta(2\theta) \leq 40°$ is less than 1 min.

(5) Magnification of the optical system is about 100 times on the TV monitor.

(6) The sample position can be adjusted precisely during the measurement by moving the furnace.

The developed system can be employed to investigate the phase relation at high-temperatures, crystal growth from a melt and kinetic analysis in phase transition.

References

[1] T.Yamanaka : X-ray powder diffraction analysis for material science (*Kodansya Scientific*, 1993) 133

[2] J.Miyahara, K.Amamiya, T.Matsusita, *Butsuri*,25(1990)398

[3] G.C.Giessen and G.E.Gordon, *Science,* 159(1968)973

[4] T.Fukumachi, S.Hosoya and O.Terasaki, J.Appl.Cryst. 6(1973)117

[5] I.Kimura and E.Sakai : Handbook of a radiation mesurements (*Daily Industrial newspaper Co.* 1989)

[6] T.Yamanaka : X-ray powder diffraction analysis for material science (*Kodansya Scientific* 1993) 71

[7] T.Izumi, *Phys. Status Solidi.* (a), 21(1979)79

[8] H.Hasizume, *Appl. Phys. Lett.*, 21(1979)84

[9] Y.Oyama, M.Hasegawa, and H.Takei, *Jpn. J. Appl. Phys.* 33 (1994) 4779.

[10] Y.Oyama, M.Hasegawa and H.Takei, *J. Cryst. Growth* 143(1994)200

[11] T.Suzuki, K.Yumoto, M.Hasegawa and T.Takei, Advances in superconductivity VII, Eds. K. Yamamoto and T.Morishita, Springer-Vlg. 1(1995) 321

[12] Y.Inatomi and K. Kuribayashi, *J. Crystal Growth,* 99 (1990)124

[13] T.Kashiwagi : Visble streams (1987) vol. 7, 25

[14] H.Komatsu, Y.Kato, S.Miyashita, T.Inoue and S.Hayashi, *Physica C* 190(1991)14

[15] K.Makita, M.Nishihara : Techniques of a high pressure fluid, (*Maruzen*, 1992)149

[16] T.Suzuki, K.Yumoto, M.Hasegawa and T.Takei, *J Cryst. Growth*, in press.

Chapter 3.

Phase relations of Bi- and Bi(Pb)-based oxide superconductors

3.1 Introduction

As mentioned in Chapter 1, the Bi-based superconductors are very important materials because of the high applicability to the superconducting industrial materials, such as high Tc, high Hc, low toxicity and cheaper starting materials. Accordingly, a large number of studies about the Bi- and Bi(Pb)-based superconductors for the powder making process [1], phase relations [2], single crystal growth [3], physical characterizations [4] and others [5,6] have been carried out. The Bi-based superconductors were discovered to replace the Sr-ion to the Ca-ion in the Bi-Sr-Cu-O system by Maeda et. al.[7]. $Bi_2Sr_2CuO_6$ (Bi-2201), $Bi_2Sr_2CaCu_2O_8$ (Bi-2212) and $Bi_2Sr_2Ca_2Cu_3O_{10}$ (Bi-2223) have been well-known in the Bi-based superconductor's family. Tc of Bi-2201 and Bi-2212 are about 7~40 and 80K, respectively. They are easy to be synthesized by calcination difficult to be grown as single crystals[8]. On the other hand, the single phase material of Bi-2223 is very difficult to synthesize, even though it has the highest Tc of about 107K. The difficulty is attributable to its incommensurate modulated structure along the a- or b-axis[9]. In order to overcome it, the Bi(Pb)-based superconductors have been developed by replacing a part of Bi-ions by the Pb-ions [10]. The Main Pb-substituting effects were as follows ; (1) disappearing

of the incommensurate, modulated structure; (2) easier making of the single phase; and (3) decreasing of sintering time.

The phase diagrams in these superconductors systems are well expected to be very complex and difficult to be established because of the 5 or 6 component elements which have a tendency to become the ease of amorphous by quenching from the melt. Accordingly, many phase diagrams different from each other have been reported by many researchers, such as Komatsu et al. [11], P. Strobel et al. [12], T. Hasegawa et al. [13] and others [14]. The essential points, such as the liquid lines and incongruent melting points, of the phase relations in these studies were mostly inconsistent. Most of these phase diagrams have been decided by the quenching methods but as mentioned in Chapter 1, the liquid phase composition at high temperature changes easily by quenching. These situations leads to the thought that the in-situ observation should be required to establish the precise phase diagram at high-temperature.

In this chapter, the pseudo-binary phase diagrams in the Bi_2SrO_4-$SrCuO_2$, $Bi_2Sr_2CuO_6$-$CaCuO_2$ and $(Bi_{0.8}Pb_{0.2})_2Sr_2CuO_6$-$CaCuO_2$ system are clarified. The phase diagram in the Bi_2SrO_4-$SrCuO_2$ system, which has not been reported in spite of the fundamental (basic) system of the Bi-based superconductors, is clarified for the first time. It was determined on heating process by the in-situ observation apparatus of HT-XPD with PSPC and optical microscope simultaneously which has already been described in Chapter 2. In addition, the effect of Ca and Pb substitution on the phase relations is also clarified and

discussed.

3.2 Sample preparation

Figure 3.1 shows triangle phase diagrams in the Bi-Sr-Cu-O, Bi-Sr-Ca-Cu-O and $(Bi_{0.8}Pb_{0.2})$-Sr-Ca-Cu-O systems. The open circles mean the sample composition in this study. The pseudo-binary line of Bi_2SrO_4-$SrCuO_2$ including Bi-2201, $Bi_2Sr_3Cu_2O_x$ (Bi-2302) and $Bi_2Sr_4Cu_3O_x$ (Bi-2403) has been firstly investigated because these oxides are counterparts to the high-Tc Bi-based superconductors, such as Bi-2201, Bi-2212 and Bi-2223 in the $Bi_2Sr_2CuO_6$-$CaCuO_2$ system. As the composition of Bi-2403 is not terminal, single phase, the stable $Bi_4Sr_8Cu_3O_x$ (Bi-4805) phase, which is close to Bi-2403 in composition, was used alternatively. The Pb substitution ratio was fixed at 0.2 because the established XPD pattern of $(Bi_{0.8}Pb_{0.2})_2Sr_2Ca_2Cu_3O_{10}$ (Bi(Pb)-2223) has been already reported elsewhere. In this study, the investigation has been performed on the $(Bi_{0.8}Pb_{0.2})_2Sr_2CuO_6$- $CaCuO_2$ system including Bi(Pb)-2201, Bi(Pb)-2212 and Bi(Pb)-2223.

Nominal compositions of the starting mixture and sintering conditions are listed in Table 3.1. Each mixture of the raw materials Bi_2O_3, PbO, $SrCO_3$, $CaCO_3$, CuO (all ; 3N) was sintered in an Al_2O_3 crucible in air. Some samples were pressed hydrostatically at $1t/cm^2$ into a rod of about 8mm diameter because of their low reactivity. The pressed samples are indicated as (p) in Table 3.1. All prepared powders were detected by XPD ($3<2\theta<70°$).

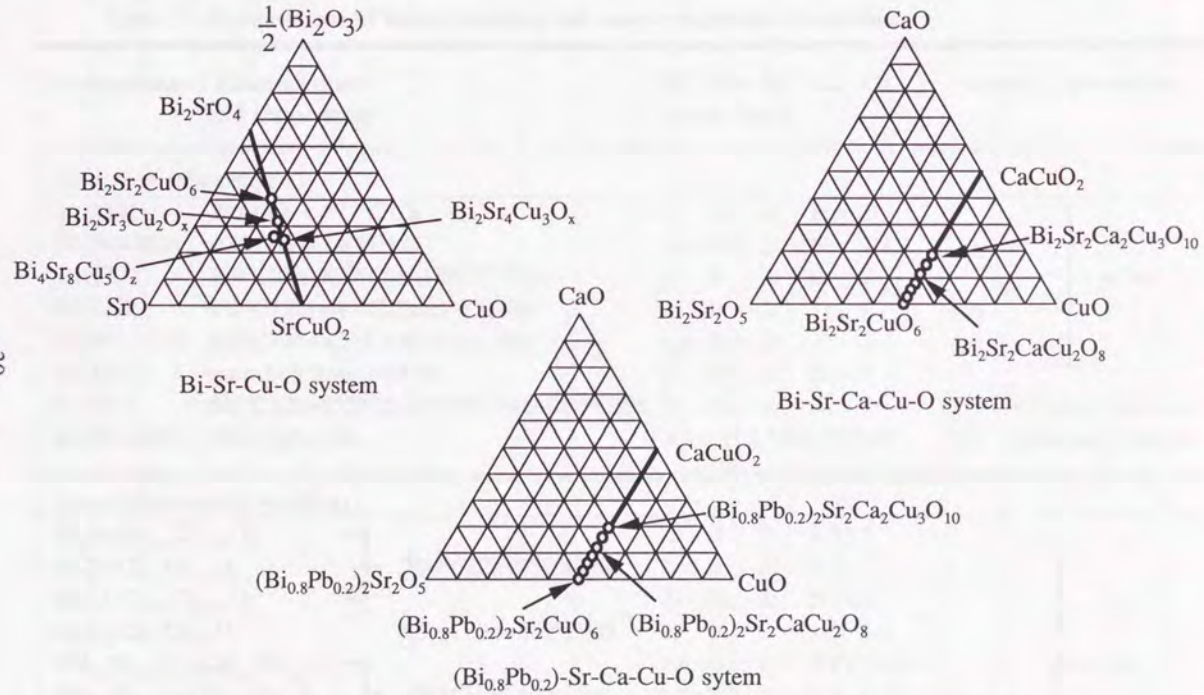

Figure 3.1 Ternary phase diagrams in the Bi-Sr-Cu-O, Bi-Sr-Ca-Cu-O and $(Bi_{0.8}Pb_{0.2})$-Sr-Ca-Cu-O systems.

Table 3.1 Compositions of starting mixture and sample preparation conditions.

Composition	Sintering time and temperature	Bi: Pb: Sr: Ca: Cu (metal ratio)	pressed	atmosphere
(stoichiometric samples)				
Bi-2201	790°C6h + 837°C12h	2: 0: 2: 0: 1		in air
Bi(Pb)-2201	800°C6h + 840°C12h	1.6: 0.4: 2: 0: 1		in air
Bi-2302	790°C24h+870°C36h+865°C120h	2: 0: 3: 0: 2		in air
Bi-2212	790°C12h+840°C12h+840°C48h	2: 0: 2: 1: 2	(p)	in air
Bi(Pb)-2212	800°C12h+820°C12h+820°C48h	1.6: 0.4: 2: 1: 2	(p)	in air
Bi-4805	quenched from 1000°C	2: 0: 3: 0: 2		in air
Bi-2223	800°C12h+855°C24h+875°C24h+880°C60h	2: 0: 2: 2: 3	(p)	92%Ar-8%O_2 in Au tube
Bi(Pb)-2223	850°C60h+90h	1.85:0.35:1.90:2.05:3.05	(p)	92%Ar-8%O_2 in Au tube
(non-stoichiometric samples)				
$Bi_2Sr_2Ca_{0.25}Cu_{1.25}O_x$	790°C12h+830°C48h	2: 0: 2: 0.25:1		in air
$Bi_2Sr_2Ca_{0.5}Cu_{1.5}O_x$	790°C12h+830°C48h	2: 0: 2: 0.5: 1		in air
$Bi_2Sr_2Ca_{0.75}Cu_{1.75}O_x$	790°C12h+830°C48h	2: 0: 2: 0.75:1		in air
$Bi_2Sr_2Ca_{1.5}Cu_{2.5}O_x$	800°C12h+860°C48h	2: 0: 2: 1.5: 2.5		in air
$(Bi_{0.8}Pb_{0.2})_2Sr_2Ca_{0.25}Cu_{1.25}O_x$	800°C12h+840°C48h	1.6: 0.4: 2: 0.25 1.25		in air
$(Bi_{0.8}Pb_{0.2})_2Sr_2Ca_{0.5}Cu_{1.5}O_x$	800°C12h+840°C48h	1.6: 0.4: 2: 0.5: 1.5		in air
$(Bi_{0.8}Pb_{0.2})_2Sr_2Ca_{0.75}Cu_{1.75}O_x$	800°C12h+840°C48h	1.6: 0.4: 2: 0.75 1.75		in air
$(Bi_{0.8}Pb_{0.2})_2Sr_2Ca_{1.5}Cu_{2.5}O_x$	850°C24h	Bi(Pb)-2212 and Bi(Pb)-2223 mix powder		in air

Each stoichiometric sample is prepared by sintering in the most appropriate temperature with soaking time. For example, the powder of $Bi_2Sr_2CaCu_2O_x$ (Bi-2212) was sintered at 795°C for 12h and then at 845 °C for 24h+24h. It had a high crystallinity and was of single phase. Since the sample had a tendency to deteriorate in humidity, the experiments were conducted to be carried out as soon as possible after synthesized.

As the Bi-4805 phase was not synthesized directly by sintering the stoichiometric starting mixture, the following procedure was adopted. At the first stage, sintered powders in the composition of Bi-2302 were prepared by quenching from 1000°C. Then, Bi-4805 of needle type crystals which were precipitated in the melt were separated based on their optical color and crystal habit. XPD confirmed that they were of the Bi-4805 single phase without any amorphous phases. Since it was very very difficult to prepare Bi-2223 Pb-free single phase samples, sintered specimens with the Bi-2223 composition were used instead of the Bi-2223 single phase samples. They were sintered under a 92%Ar-8%O_2 gas flow condition in an Au tube and were confirmed by XPD to be of a mixed phase of Bi-2212, Ca_2CuO_3 and few Bi-2223. As single phase samples Bi(Pb)-2223 in the stoichiometric composition of $(Bi_{0.8}Pb_{0.2})_2Sr_2Ca_2Cu_3O_{10}$ could not be synthesized, the samples synthesized from coprecipitated powders supplied from by DOWA Indust. Co. were used. They were sintered under a 92%Ar-8%O_2 gas flow condition in an Au tube to avoid an unexpected Al contamination from an Al_2O_3 crucible. The composition

of the sintered samples thus prepared was $Bi_{1.85}Pb_{0.35}Sr_{1.90}Ca_{2.05}Cu_{3.05}O_x$. Non-stoichiometric samples were prepared under the condition as shown also in Table 3.1, where the sample of $(Bi_{0.8}Pb_{0.2})_2Sr_2Ca_{1.5}Cu_{2.5}O_x$ listed at the final column of the table was prepared from the mixture of the Bi(Pb)-2212 and Bi(Pb)-2223 powders. The whole samples were confirmed to be of multi-phases by XPD.

3.3 Experimental procedure

Each powder sample was placed on the MgO plate, as mentioned in Chapter 2.3 and phase relations were determined from the changes in X-ray and visual patterns on heating runs. In the first stage, the phase relations were roughly determined on heating at 10 °C/min, and then they were precisely investigated at 0.2 to 1 °C/min around the phase change temperatures. Main phase changes were investigated by XPD and by optical observation continuously for 2~24 hours at the constant temperature around the phase changes. The heating rate before reaching the target temperature was 20 °C/min to prevent superheating. The visual observation was continuously carried out from room temperature to the end of each run. After cooling in the furnace, the sample solidified was analyzed by an electron microprobe (SEM-EPMA). In this analysis, both upper and lower parts, as well as the surface, of the sample were also analyzed.

3.4 Results and discussion

3.4.1 Bi_2SrO_4-$SrCuO_2$ system

Figure 3.2 shows the HT-XPD patterns and video pictures at each temperature in Bi-2201 and a molten state was observed at 898°C (b). Figure 3.2 (b) shows a coexisting state of the liquid and starting phase Bi-2201. A liquid state was only observed above 906°C (c).

Figure 3.3 shows the HT-XPD patterns and video pictures at each temperature in Bi-2302, and a partial melting started at 901°C (b). Figure 3.3 (b) shows a coexisting state of the liquid and starting phase Bi-2302. This coexisting region was observed in the temperature between 901 and 913°C. The XPD analysis identified that the phase was of Bi-4805 + $SrCuO_2$ + L as shown in Figure 3.3 (c). The video pictures of this state revealed that needle and platelet crystals floated on the liquid surface. Such a region was observed between 913 and 923°C. From the XPD patterns in Figure 3.3 (d) was the state at 925°C identified to be of $SrCuO_2$+L. The video picture at 925°C shows needle type crystals on the molten surface and this region was found to be stable in the wide temperature between 923 and 1010°C. Complete melting was detected above 1010°C.

Figures 3.4 and 3.5 show the HT-XPD patterns and video pictures between 880 and 952°C, respectively when heated continuously at a rate of

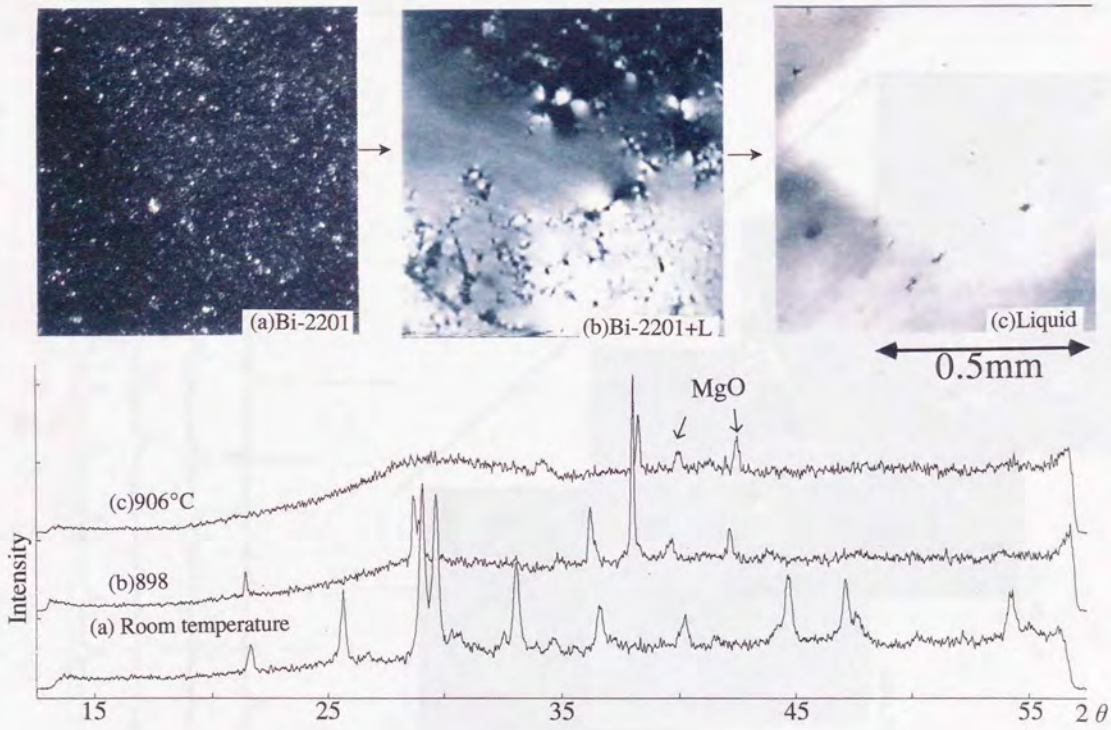

Figure 3.2 HT-XPD patterns and video pictures at each temperature of Bi-2201.
Each XPD pattern was identified as follows; (a) Bi-2201 (b)Bi-2201+L (c) Liquid.

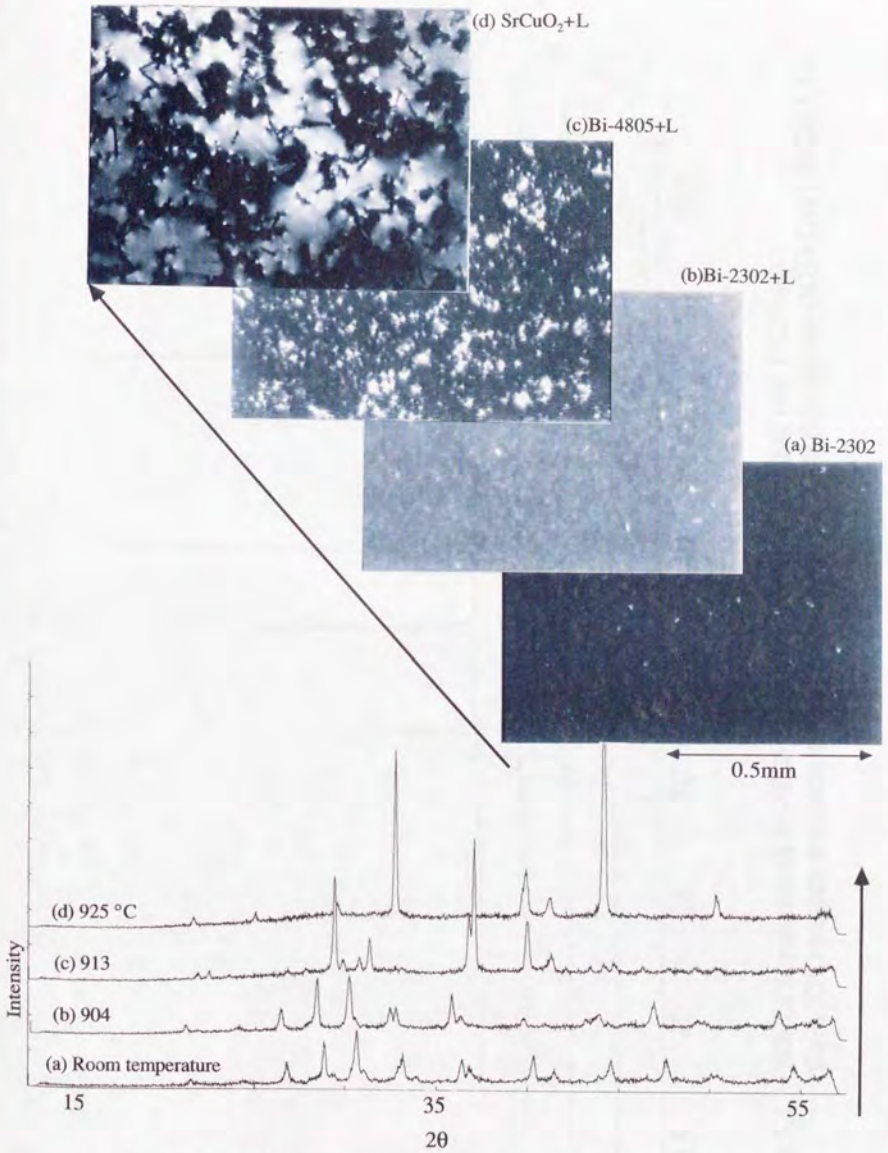

Figure 3.3 HT-XPD patterns and video pictures at each temperature of Bi-2302. Each XPD pattern was identified as follows; (a) Bi-2302 (b)Bi-2302+L (c)Bi-4805+L (d) $SrCuO_2$+L

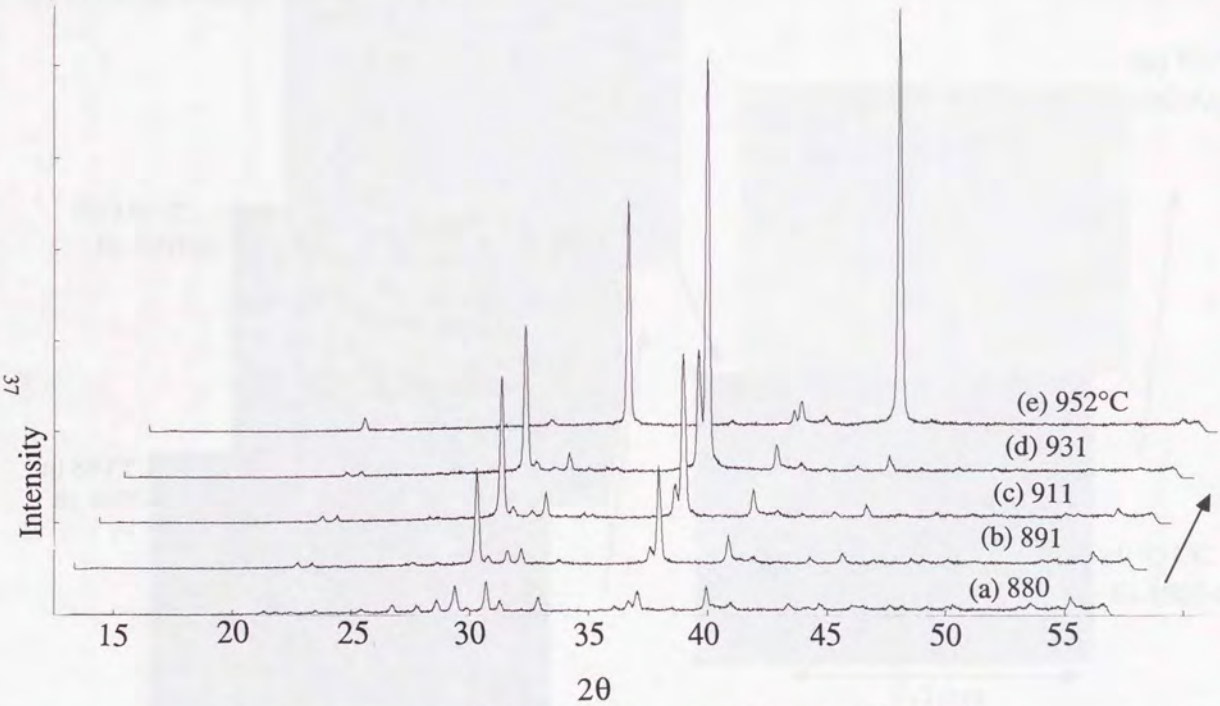

Figure 3.4 HT-XPD patterns of Bi-4805 at each temperature (heating rate 1°C/min).
Each XPD pattern was identified as follows; (a) Bi-4805 (b)~(d) Bi-4805+L (e) $SrCuO_2$+L.

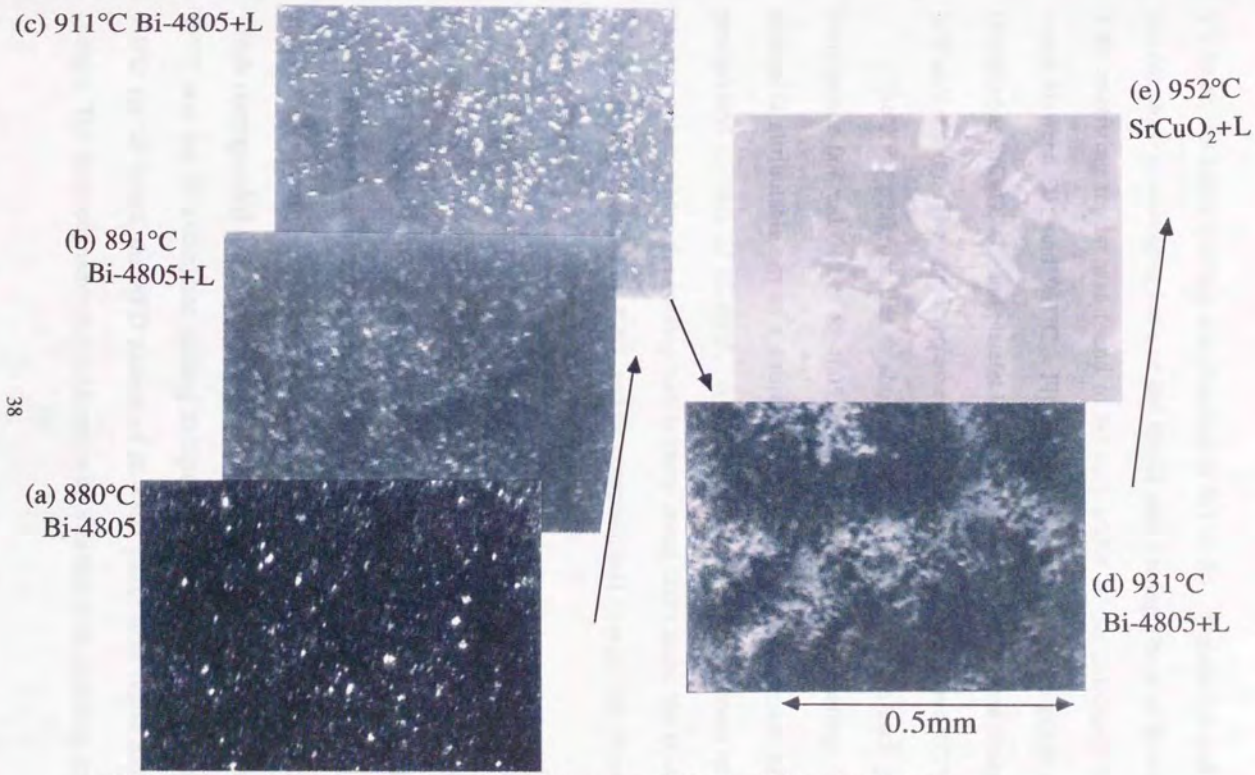

Figure 3.5 Video pictures corresponding to each X-ray diffraction pattern.

1°C/min. An initial melting was observed at 891°C (b). Figures 3.4 and 3.5 (b)~(d) show a coexisting state of the liquid and starting phase of Bi-4805. This coexisting region was found to be very stable in the extremely wide range between 891 and 951°C. Figure 3.4 (e) shows that the phase was identified as $SrCuO_2$ +L, and platelet large crystals in the liquid were observed in Figure 3.5 (e). The sample became a complete melting state above 977°C.

The XPD peak profiles as shown in Figure 3.4 (d), where each peak corresponds *00l* and *0k0* of Bi-4805, changed gradually with heating. This change is attributable not to a structure transition, but an alignment of the precipitated crystals of Bi-4805. After quenched by shutting-down of the furnace power where the cooling rate became about 200°C/min, the Bi-4805 phase was only detected by XPD, and no compositional change was observed by SEM-EPMA.

The variation in the amount of liquid in the Bi-4805 sample was shown in Figure 3.6. After partial melting at 891°C, the amount of liquid increased up to 902°C, and it decreased rapidly with increasing temperature up to 910°C. Further heating brought about an increase in liquid again between 910 and 952°C gradually, and then rapid increase was observed at about 952°C, which corresponded to a decomposition to $SrCuO_2$+L. The final increase at 977°C was due to a complete melting to liquid. In the experiment holding at 910°C for 24 hours, the XPD pattern of Bi-4805 phase with liquid did not change. The thermodynamical consideration implies that such a melting state

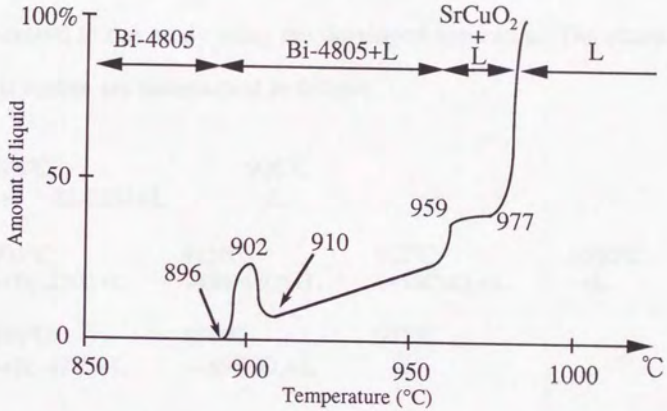

Figure 3.6 Variation of liquid phase with heating in Bi-4805 sample at a heating rate of 1°C/min.

should not be stable because a solid phase exists at a higher temperature region above the liquid phase. Therefore, the decrease around 910°C might be attributable to the re-crystallization and the first increase may correspond to the melting of weak-bonded or amorphous part around the grain boundary. Sintered sample has generally large amount of such a part. Such a phenomenon was first discovered in this study using the developed apparatus. The phase relations in this system are summarized as follows,

	898°C		906°C	
Bi-2201	→ Bi-2201+L		→L	
	901°C	913°C	923°C	1010°C
Bi-2302	→Bi-2302+L	→Bi-4805+L	→$SrCuO_2$+L	→L
	891°C	951°C	977°C	
Bi-4805	→Bi-4805+L	→$SrCuO_2$+L	→L	

From these results, the phase relation in the Bi_2SrO_4-$SrCuO_2$ system can be drawn as Figure 3.7. This pseudo-binary phase diagram in the Bi_2O_3-SrO-CuO ternary system is a first report among the numerous studies on Bi-Sr-Ca-Cu-O. It became clear that the coexisting states of starting solid phase and liquid were observed widely between 10~60°C, the incongruent melting point became higher with increasing $SrCuO_2$ concentration. Liquidus line at the composition of Bi-4805 was lower than that at Bi-2302 composition. This lowering is attributable to a less content of Cu in Bi-4805 which was used as a representative of Bi-2403 (Bi-4806).

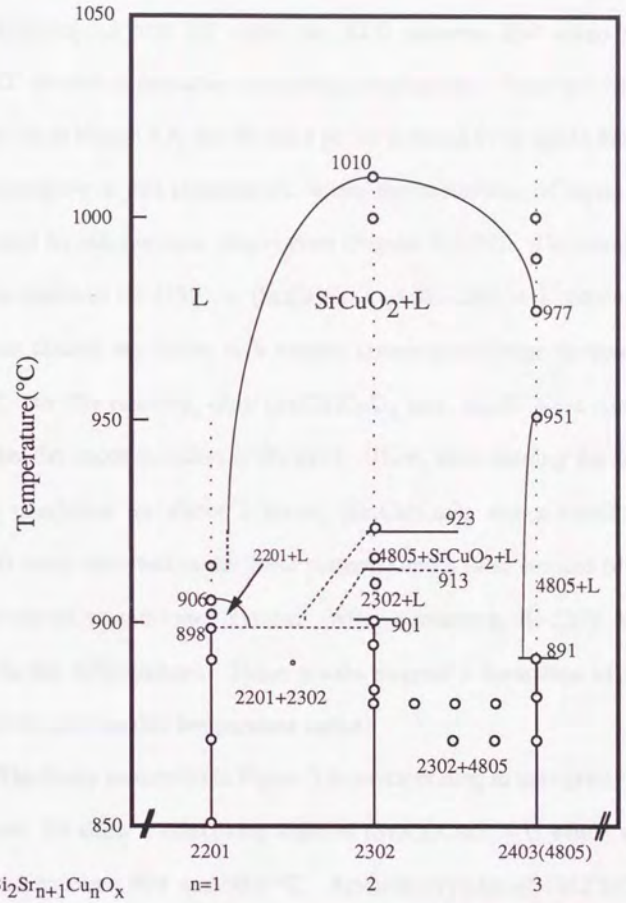

Figure 3.7 Pseudo-binary phase diagram in the Bi_2SrO_4-$SrCuO_2$ system.
Broken lines show successive mesurements on heating.
Open circles mean experimental data at fixed temperatures.
Each label means as follows.
2201:$Bi_2Sr_2CuO_6$ 2302:$Bi_2Sr_3Cu_2O_8$
4805:$Bi_4Sr_8Cu_5O_x$

2.4.2 $Bi_2Sr_2CuO_6$-$CaCuO_2$ system

Figures 3.8 and 3.9 show the XPD patterns and video pictures of Bi-2212 at each temperature in heating, respectively. From the XPD patterns (a) and (b) in Figure 3.8, the Bi-2212 phase is found to be stable below 887 °C and decompose at this temperature, where the occurrence of liquid phase was confirmed by microscopic observation (Figure 3.9 (b)). The results indicate that the reaction Bi-2212 $\rightarrow$ (Sr,Ca)CuO_2 + Bi-2201 + L proceeds. The resultant phases are stable in a narrow temperature range between 887 and 894 °C. In this reaction, only (Sr,Ca)CuO_2 and liquid were first observed just after the decomposition of Bi-2212. Then, after holding the temperature at this condition for about 2 hours, (Sr,Ca)CuO_2 and a small amount of Bi-2201 were observed in the XPD patterns; and a little amount of liquid was also observed in the video system. After quenching, Bi-2201 was a main phase in the XPD pattern. These results suggest a formation of amorphous state of Bi-2201 in this temperature range.

The X-ray pattern (c) in Figure 3.8 corresponding to the optical photograph in Figure 3.9 show a coexisting state of (Sr,Ca)CuO_2 + L which was widely observed between 894 and 955 °C. Acicular crystals of (Sr,Ca)CuO_2 were often found on the liquid surface. The lattice constants of the precipitated crystals at the temperature between 887 and 910 °C obtained from the XPD were almost comparable with those of $(Sr_{0.6}Ca_{0.4})CuO_2$, JCPDS Card No. 42-534, considering with the thermal expansion. On the other hand, the

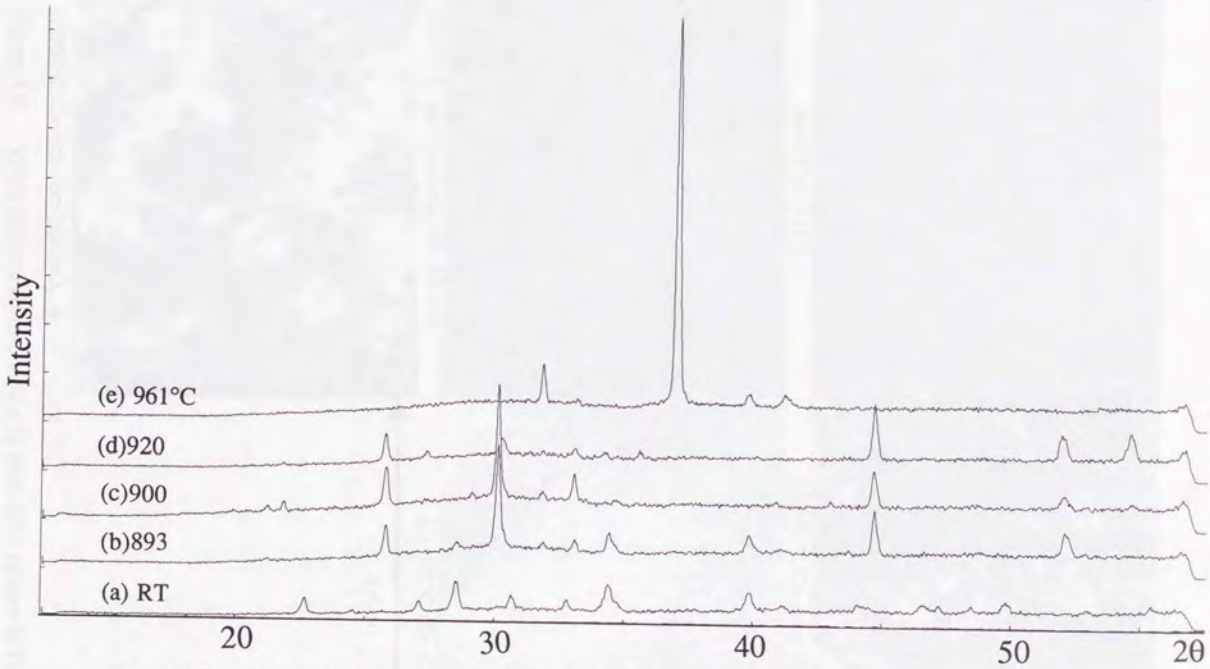

Figure 3.8 HT-XPD patterns of Bi-2212 at each temperature.
Each XPD pattern was identified as follows; (a) Bi-2212 (b) (Sr,Ca)CuO_2+Bi-2201+L (c) Ca-rich (Sr,Ca)CuO_2 +L (d) Ca-poor (Sr,Ca)CuO_2+L (e) (Sr, Ca)O+L.

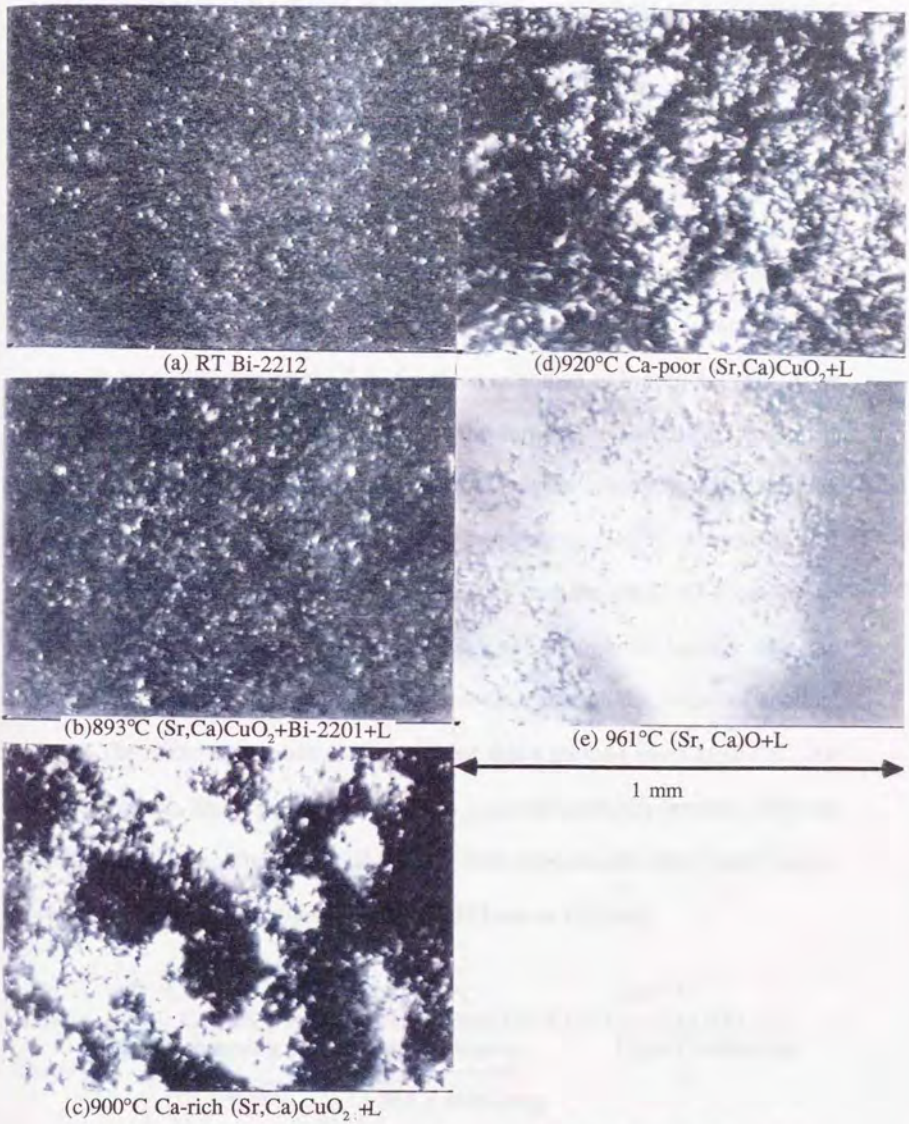

Figure 3.9 Video pictures corresponding to each XPD pattern in Figure 3.8.

pattern in Figure 3.8 (d) was assumed to be a compound of calcium-poor $(Sr,Ca)CuO_2$ because the lattice constants were almost equivalent to those of $SrCuO_2$, JCPDS Card No. 39-1492, considering with the thermal expansion. The needle-like crystals became plates at 920°C as shown in Figure 3.9 (d). The change in Ca concentration was observed between 887 and 955 °C, and was also confirmed by the compositional analysis by EPMA after quenching. The (Sr,Ca)O + L phase as finally observed above 955 °C, where acicular crystals were observed on the liquid surface as shown in Figure 3.9 (e). After quenching by cutting off the current of the furnace, the solidified specimen was inspected by XPD and SEM-EPMA, but no trace (Sr,Ca)O besides $(Sr,Ca)CuO_2$ was detected. On cooling from above 960°C, a formation of $(Sr,Ca)CuO_2$ phase was observed near and around the (Sr,Ca)O phase by an optical microscope. Accordingly, (Sr,Ca)O is thought to become into the $(Sr,Ca)CuO_2$ with a solid-melt reaction and disappear on the period of cooling.

The microscope observation revealed that a melting starts at 887°C. An amount of the liquid phase was found to increase gradually between 894 and 955 °C, and then abruptly around 955°C. This indicates that the phase changes at the stoichiometric composition of Bi-2212 are as follows:

$$\underset{\text{Liquid increasing}}{\overset{887\ ^\circ C}{\text{Bi-2212}}} \rightarrow (Sr,Ca)CuO_2 + \text{Bi-2201} + L \underset{\text{Liquid increasing}}{\overset{894\ ^\circ C}{\rightarrow}} (Sr,Ca)CuO_2 + L \underset{\text{Liquid increasing}}{\overset{955\ ^\circ C}{\rightarrow}} (Sr,Ca)O + L.$$

$$\xrightarrow[\text{Sr/Ca increasing}]{}$$

Figures 3.10 and 3.11 show the XPD patterns and video pictures of the Bi-2223 composition sample at each temperature, respectively. A coexistence of Bi-2212, Ca_2CuO_3 and a little Bi-2223 at room temperature was identified by XPD (Figure 3.10 (a)). The formation of the liquid phase was confirmed by the microscopic observation at 950°C (Figure 3.11 (b)). An apparent segregation of solid from liquid was also observed in this picture. As shown in the patterns (b) in Figures 3.10 and 3.11, the coexisting state of the phase $(Sr,Ca)CuO_2$ with L, was observed between 896 and 930°C. These results indicate that all of the starting phases decompose and phase changes at 896°C. The patterns (c) in Figure 3.10 and 3.11 were identified as $(Sr,Ca)_2CuO_3$+L. Any visual differences between $(Sr,Ca)CuO_2$ + L and $(Sr,Ca)_2CuO_3$+L were not observed. The $(Sr,Ca)_2CuO_3$+L phases were observed between 930 and 960°C. Finally, (Sr,Ca)O+L phases appear above 960°C, where acicular crystals were observed on the liquid surface as shown in Figure 3.11 (d). $(Sr,Ca)_2CuO_3$ and $(Sr,Ca)CuO_2$ crystals showed a decrease in XPD intensity when keeping for a few hours in the atmosphere, suggesting deterioration of crystallinity, and often disappeared in XPD on quenched samples which the precipitated phase was detected at high temperature.

The amount of the liquid phase was found to increase gradually between 896 and 955 °C, and then abruptly at around 955 °C. These results indicate that the phase changes at the stoichiometric composition of Bi-2223 are as follows:

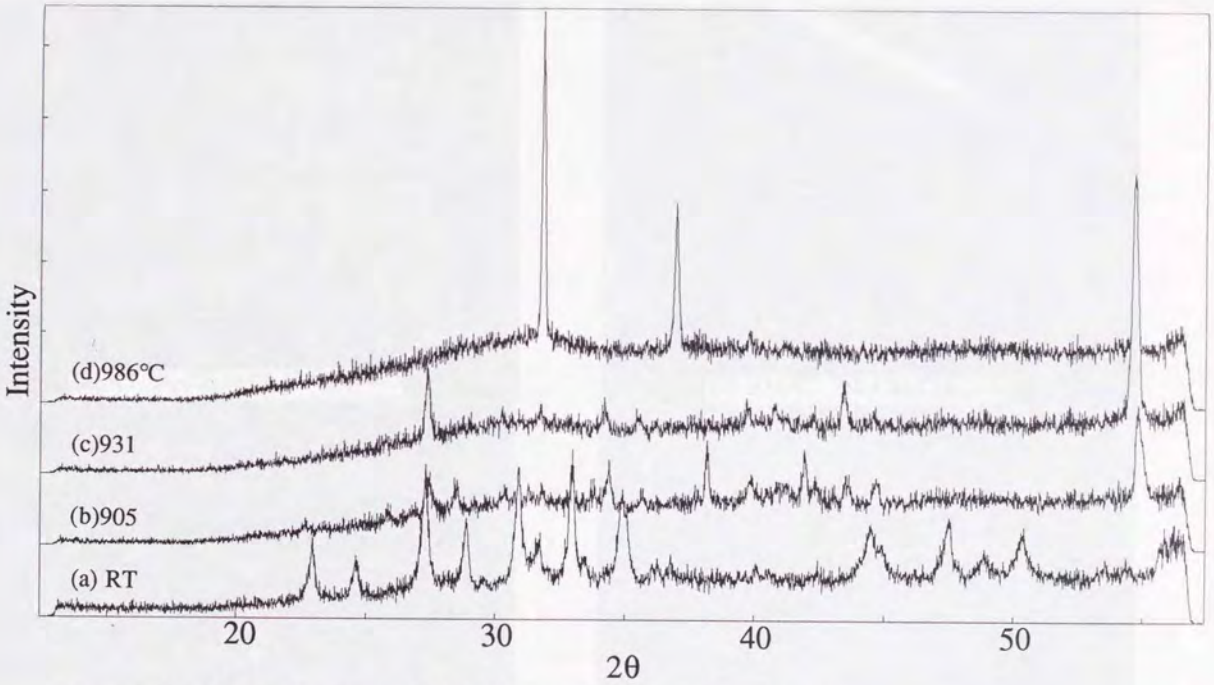

Figure 3.10 HT-XPD patterns of Bi-2223 composition at each temperature.
Each XPD pattern was identified as follows; (a) Bi-2212+Ca_2CuO_3+2223+L (b) (Sr,Ca)CuO_2+L (c) $(Sr,Ca)_2CuO_3$+L (d) (Sr, Ca)O+L.

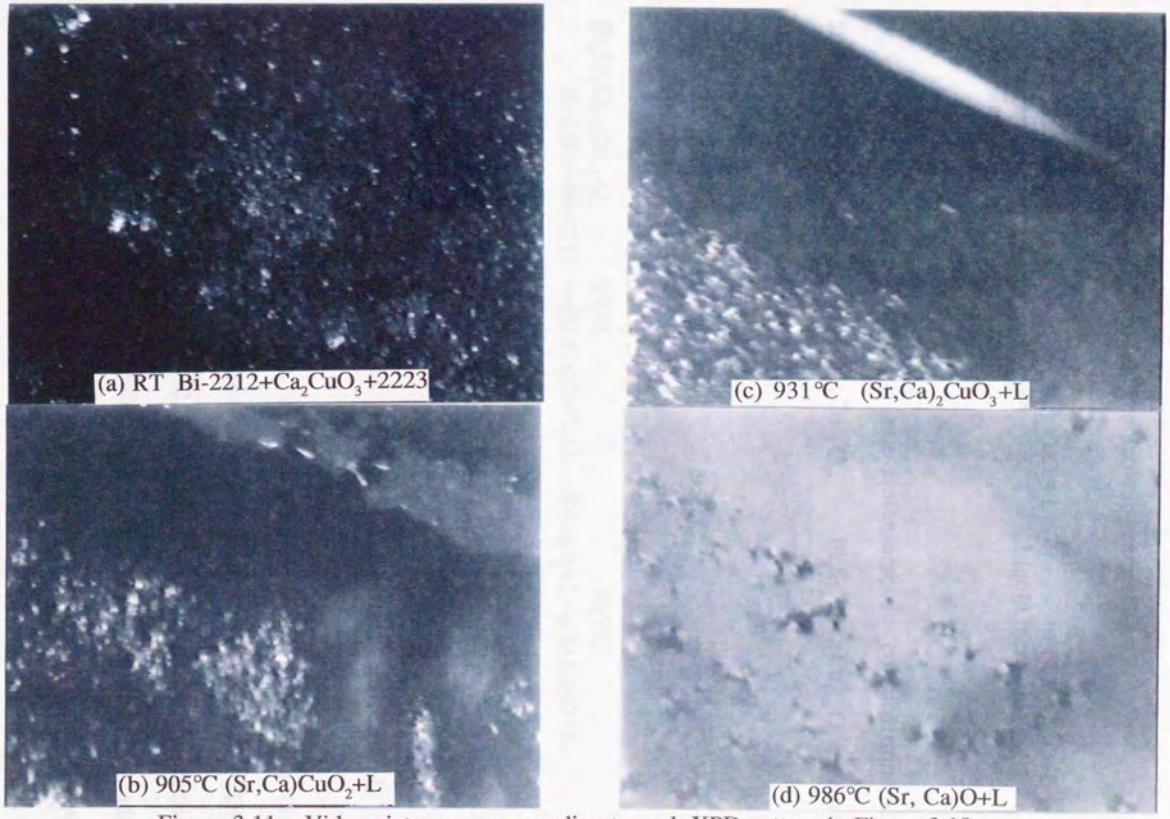

Figure 3.11 Video pictures corresponding to each XPD pattern in Figure 3.10.

$Bi\text{-}2212+Ca_2CuO_3+Bi\text{-}2223$(Bi-2223 composition sample)→

896°C 930°C 960°C
→$(Sr,Ca)CuO_2$+L → $(Sr,Ca)_2CuO_3$+L → (Sr,Ca)O+L
Gradually liquid increasing Liquid increasing

The phase changes at the non-stoichiometric compositions of $Bi_2Sr_2Ca_{0.25}Cu_{1.25}O_x$, $Bi_2Sr_2Ca_{0.5}Cu_{1.5}O_x$, $Bi_2Sr_2Ca_{0.75}Cu_{1.75}O_x$ and $Bi_2Sr_2Ca_{1.5}Cu_{2.5}O_x$ were as follows,

$Bi_2Sr_2Ca_{0.25}Cu_{1.25}O_x$ 895°C 956°C
Bi-2201+Bi-2212 →$SrCuO_2$+L →L

$Bi_2Sr_2Ca_{0.5}Cu_{1.5}O_x$ 892°C 960°C
Bi-2201+Bi-2212 →$(Sr,Ca)CuO_2$+L→$SrCuO_2$+L→(Sr,Ca)O+L

$Bi_2Sr_2Ca_{0.75}Cu_{1.75}O_x$ 889°C 960°C
Bi-2201+Bi-2212 →$(Sr,Ca)CuO_2$+L→$SrCuO_2$+L→(Sr,Ca)O+L

$Bi_2Sr_2Ca_{1.5}Cu_{2.5}O_x$ 887°C 952°C 960°C
Bi-2212+$(Sr,Ca)CuO_2$→$(Sr,Ca)CuO_2$+L →$(Sr,Ca)_2CuO_3$+L →(Sr,Ca)O+L

To summarize the results, a pseudo-binary phase diagram in the $Bi_2Sr_2CuO_6$-$CaCuO_2$ system is illustrated as shown in Figure 3.12. The incongruent melting point of Bi-2212 was the lowest in the stoichiometric oxides. The positively inclined liquidus line is drawn above 900°C. It should be noted that the phase diagram obtained in this study is extremely different from that by Komatsu et al., as shown in Figure 3.13[11], where the positive

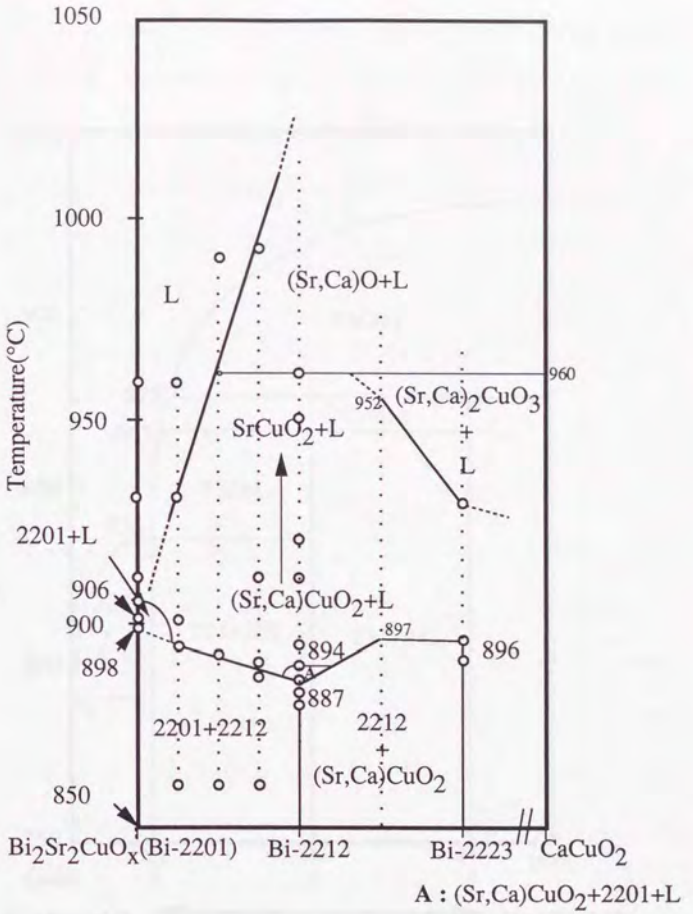

Figure 3.12 Pseudo-binary phase diagrame in the $Bi_2Sr_2CuO_x$-$CaCuO_2$ system.
Broken lines show successive mesurements on heating.
Open circles mean experimental data at a fixed temperature.

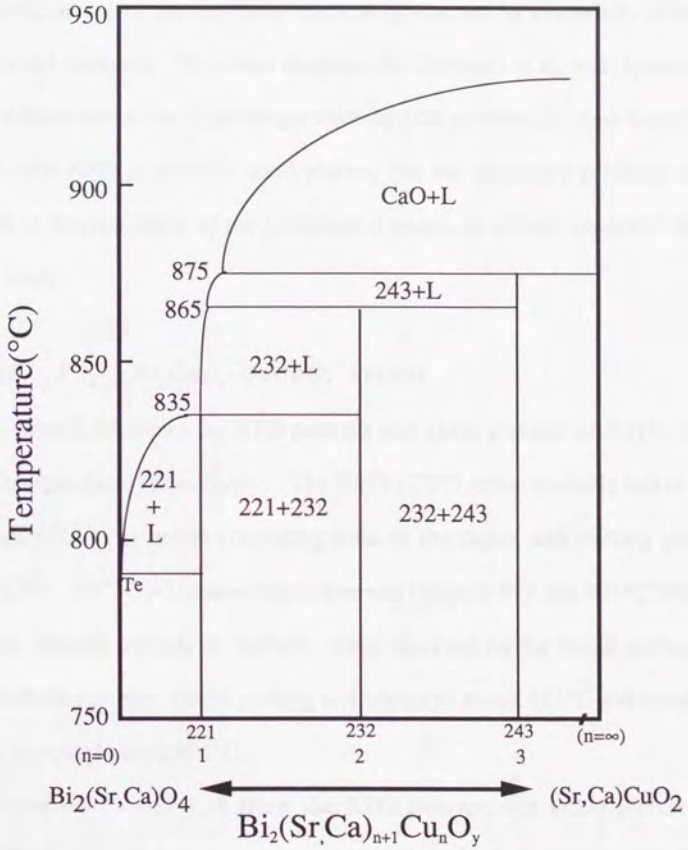

Figure 3.13 Pseudo-binary phase diagram in the $Bi_2(Sr,Ca)O_4$-$(Sr,Ca)CuO_2$ system by Komatsu et al.[11].
Each label means as follows.
221:$Bi_4(Sr,Ca)_2CuO_6$ 232:$Bi_2(Sr,Ca)_3Cu_2O_8$
243:$Bi_2(Sr,Ca)_4Cu_3O_{10}$

inclination of the liquidus curve was obtained. Thus, all of the points such as transition temperatures and phase relations are inconsistent with each other. These inconsistencies are caused by the results obtained by essentially different experimental methods. The phase diagrams by Komatsu et al. was determined by a combination of the high-temperature optical microscopy and quenching method with XPD to identify solid phases, but the quenched products often misleads in determination of the precipitated phase, as already observed in the present study.

2.4.3 $(Bi_{0.8}Pb_{0.2})_2Sr_2CuO_6$-$CaCuO_2$ system

Figures 3.14 shows the XPD patterns and video pictures of Bi(Pb)-2201 at each temperature, respectively. The Bi(Pb)-2201 phase is stable below 891 °C. Figure 3.14 (b) shows coexisting state of the liquid and starting phases Bi(Pb)-2201. $SrCuO_2$+L phases were observed between 899 and 901°C (Figure 3.13 (c)). Needle crystals of $SrCuO_2$ were observed on the liquid surface by the optical microscope. Initial melting was observed above 891°C and complete melting appeared above 906°C.

Figures 3.15 and 3.16 show the XPD patterns and video pictures of Bi(Pb)-2212 at each temperature, respectively. As indicated in the XPD patterns (a) and (b) in Figure 3.15, the Bi(Pb)-2212 phase was stable below 881 °C, which is the decomposition point of Bi(Pb)-2212. Both the XPD patterns (b) and (c) in Figures 3.15 and 3.16 indicate the reaction Bi(Pb)-2212

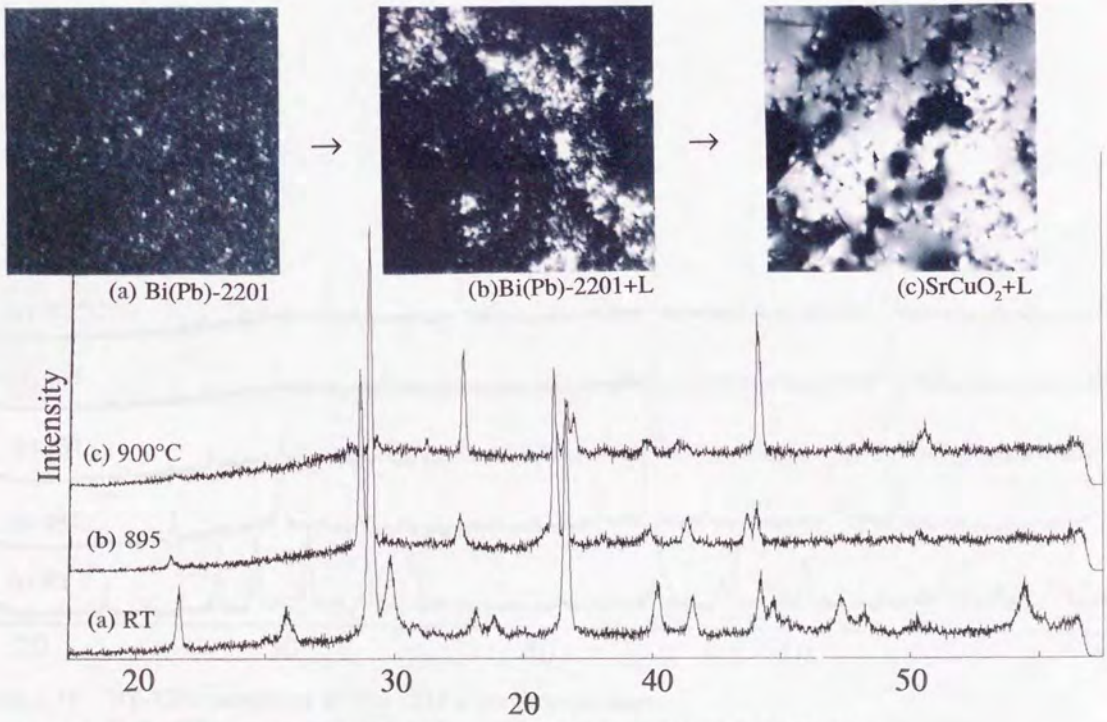

Figure 3.14 HT-XPD patterns and video picture at each temperature of Bi(Pb)-2201.
Each XPD pattern was identified as follows; (a) Bi(Pb)-2201 (b) Bi(Pb)-2201+L (c) $SrCuO_2$+L.

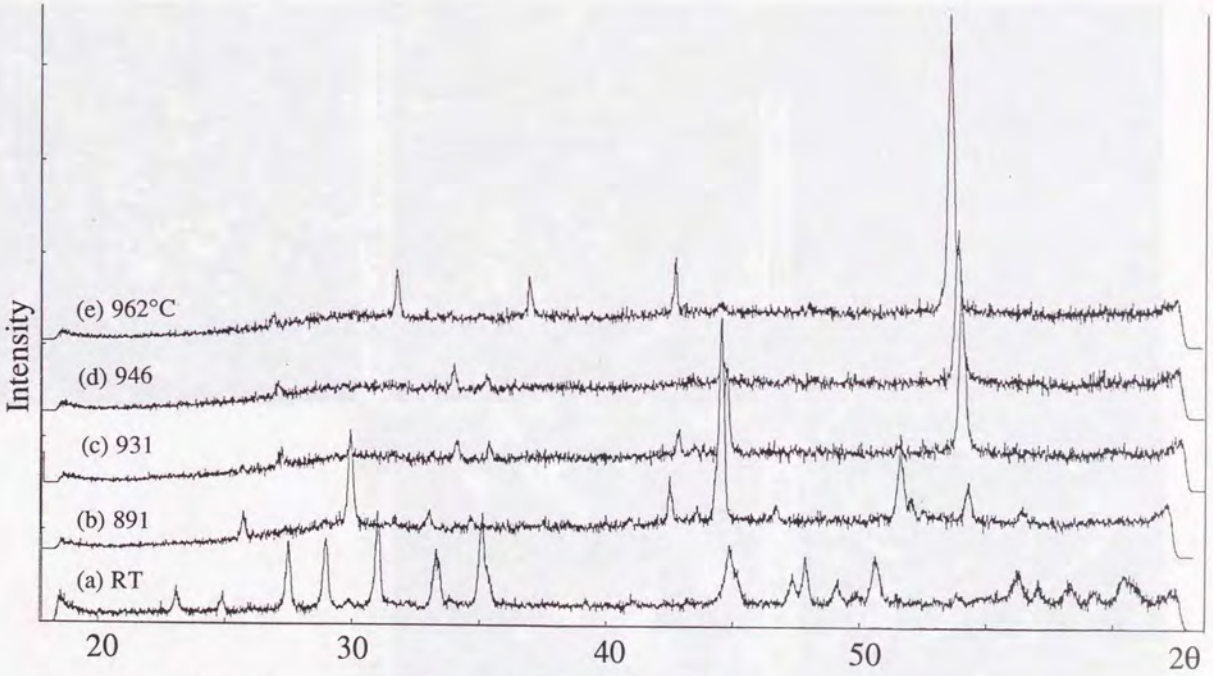

Figure 3.15 HT-XPD patterns of Bi(Pb)-2212 at each temperature.
Each XPD pattern was identified as follows; (a) Bi(Pb)-2212 (b) $SrCuO_2$+Bi(Pb)-2201+L (c) Ca-rich (Sr,Ca)CuO_2+L (d) Ca-poor (Sr,Ca)CuO_2+L (e) (Sr, Ca)O+L.

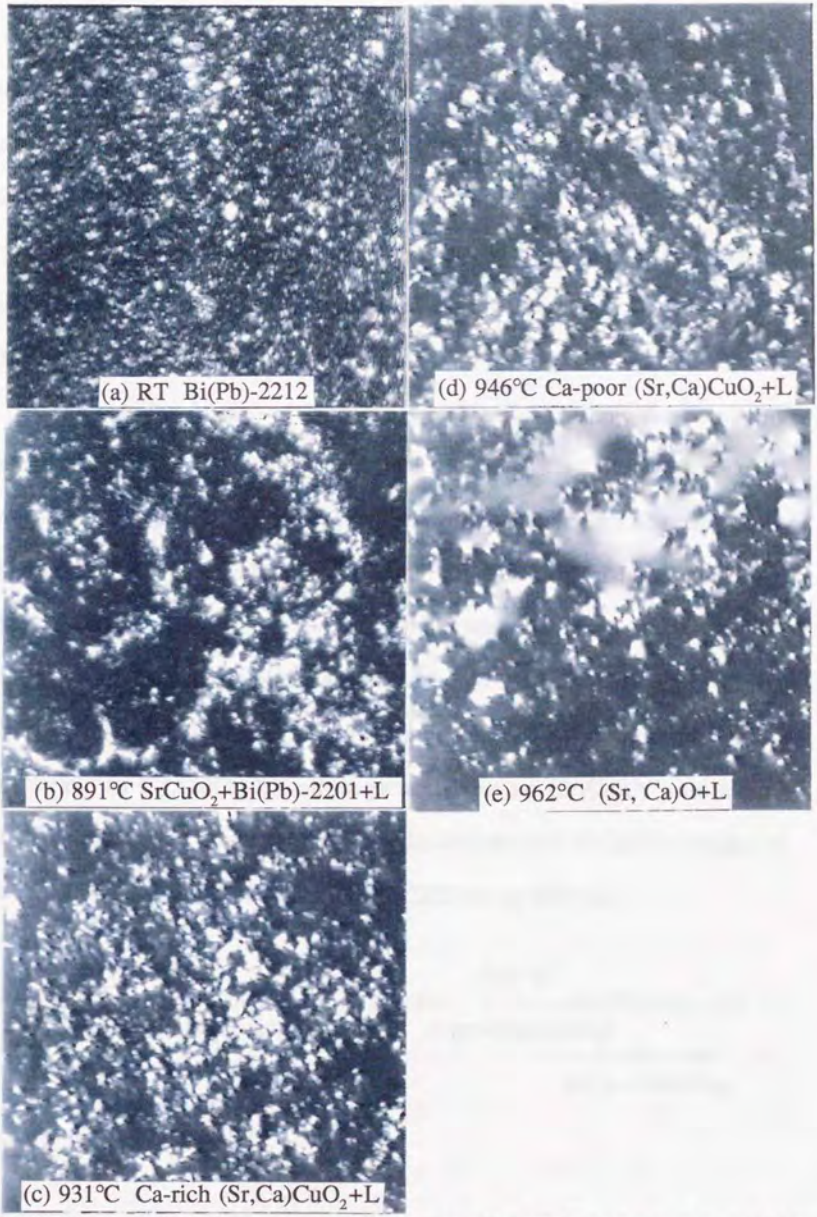

Figure 3.16 Video pictures corresponding to each XPD pattern in Figure 3.15.

$\rightarrow$ (Sr,Ca)CuO_2 + Bi(Pb)-2201 + L. The resultant phases were stable in the temperature range between 881 and 921 °C. In this reaction, only (Sr,Ca)CuO_2 and liquid were firstly observed just after the decomposition of Bi(Pb)-2212. Then, after holding at 891°C for about 2 hours, (Sr,Ca)CuO_2 and Bi(Pb)-2201 were detected by HT-XPD, and a small amount of liquid was observed by the optical microscope. Such a phenomenon was also observed in the $Bi_2Sr_2CuO_6$-$CaCuO_2$ system.

The patterns (c) and (d) in Figures 3.15 and 3.16 show the coexisting state of (Sr,Ca)CuO_2+ L., where acicular crystals of (Sr,Ca)CuO_2 were observed on the liquid surface. This state was widely observed between 920 and 960°C. Plate crystals of (Sr,Ca)CuO_2 in the liquid are observed in Figures 3.16 (c) and (d). The (Sr,Ca)O + L phase was finally observed above 960°C, and the acicular crystals are also observed on the liquid surface as shown in Figure 3.16 (e). Most of the phase relations, the habit changes, the changes in the Sr/Ca ratio in (Sr,Ca)CuO_2, and unquenchiability of (Sr,Ca)O, were almost the same as those in Bi-2212. These results indicate that the phase changes at the stoichiometric composition of Bi(Pb)-2212 are as follows:

$$\text{Bi(Pb)-2212} \xrightarrow[\text{Liquid increasing}]{881\ ^\circ\text{C}} \text{(Sr,Ca)}CuO_2\text{+Bi(Pb)-2201 +L} \xrightarrow[\text{Liquid increasing}]{920\ ^\circ\text{C}} \text{(Sr,Ca)}CuO_2\text{ + L} \xrightarrow[\text{Sr/Ca increasing}]{960\ ^\circ\text{C}} \text{(Sr,Ca)O +L.}$$

Figures 3.17 and 3.18 show the XPD patterns and video pictures of Bi(Pb)-2223 at each temperature, respectively. The XPD patterns in Figure 3.17 (a) was identified as the Bi(Pb)-2223 phase, which was decomposed at 874°C, as indicated in the pattern (b). The decomposition of the sample was observed as shown in Figure 3.18 (b). The patterns (b) in Figures 3.17 and 3.18 show the coexisting state of $(Sr,Ca)_2CuO_3$+ L. This phase was observed between 874 and 925 °C. The pattern (b) has a halo around 2θ=30~35°. However, a little amount of liquid was observed by the optical microscope. Accordingly, an amorphous phase might coexist with $(Sr,Ca)_2CuO_3$ and liquid. The composition of amorphous phase is thought to be Bi-Cu oxide because of the existence of solid state $(Sr,Ca)_2CuO_3$ in the sample. This amorphous phase gradually changed to liquid with heating up to 925°C, as shown in Figures 3.18 (b) and (c). The amorphous phase was stable on heating for about 24 hours at the incongruent melting point 896°C, as indicated in Figure 3.18 (b). The separation of solid from liquid in the melt of Bi(Pb)-2223 was observed in Figure 3.18 (c). The patterns (c) in Figures 3.17 and 3.18 were recognized as $(Sr,Ca)_2CuO_3$+ (Sr,Ca)O + L phases, which were stable between 930 and 960°C and the (Sr,Ca)O+L phase remained up to above 944°C. Acicular crystals are found on the liquid surface in Figure 3.18 (d). In the $(Sr,Ca)_2CuO_3$ and $(Sr,Ca)CuO_2$ crystals, marked deterioration in crystallinity was apparent when keeping for a few hours in air. Disappearance of these crystalline phases was observed by XPD after quenching even though detected

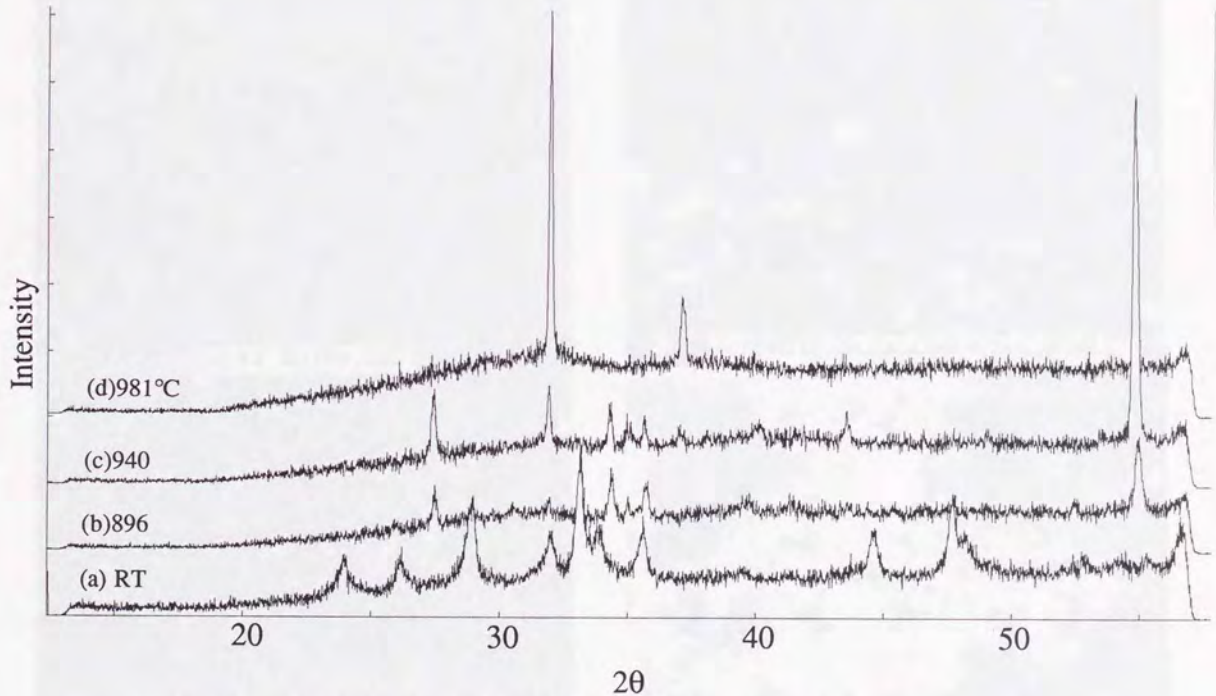

Figure 3.17 HT-XPD patterns of Bi(Pb)-2223 at each temperature.
Each XPD pattern was identified as follows; (a) Bi(Pb)-2223 (b) $(Sr,Ca)_2CuO_3$+L (c) $(Sr,Ca)_2CuO_3$+(Sr,Ca)O+L (d) (Sr, Ca)O+L.

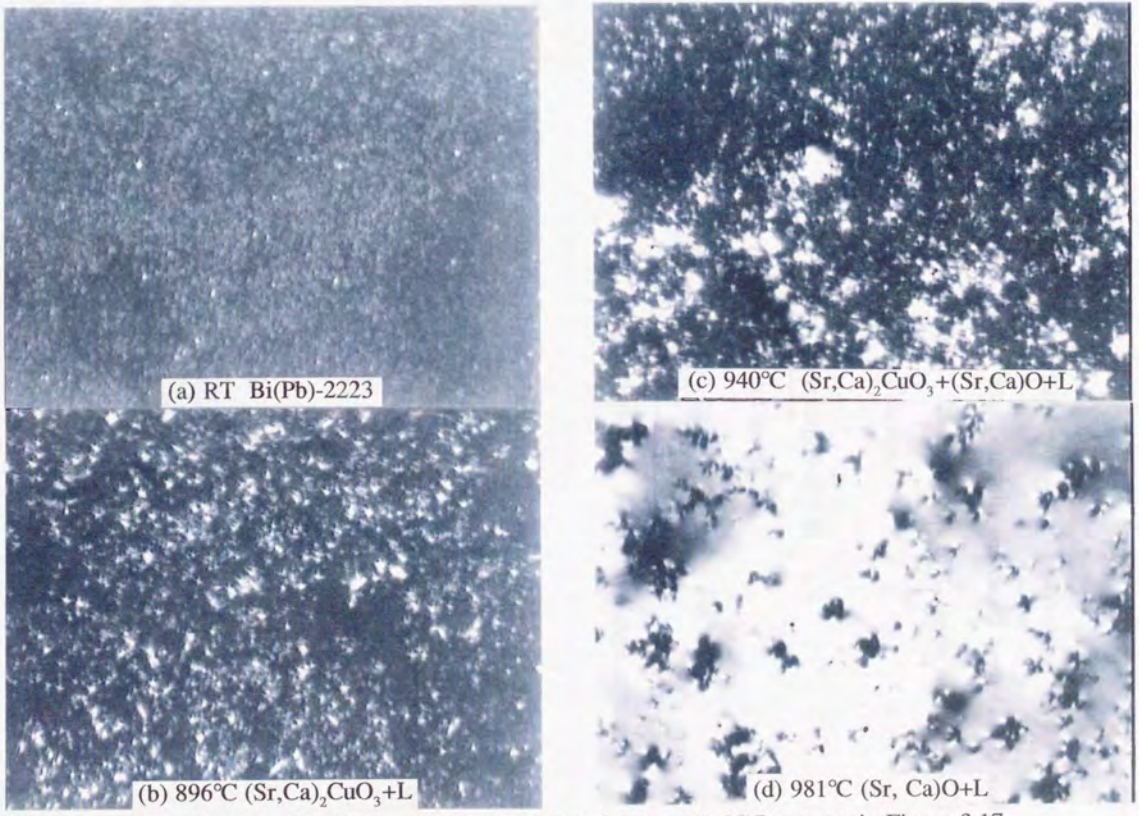

Figure 3.18 Video pictures corresponding to each XPD pattern in Figure 3.17.

at high-temperatures.

The amount of the liquid phase was found to increase very slowly between 874 and 925 °C. Then, it was gradually increased between 925 and 944°C, and abruptly around 944 °C. These results indicate an occurrence of the phase changes in Bi(Pb)-2223, as follows:

$$\text{Bi(Pb)-2223} \xrightarrow{874^{\circ}C} (Sr,Ca)CuO_2 + \text{Amorphous} + L \rightarrow$$

Gradually very slow liquid increasing

$$\rightarrow \xrightarrow{925^{\circ}C} (Sr,Ca)_2CuO_3 + (Sr,Ca)O + L \rightarrow \xrightarrow{944^{\circ}C} (Sr,Ca)O + L$$

Gradually liquid increasing rapidly liquid increasing

On the other hands, the phase relations of non-stoichiometric compositions o f $(Bi_{0.8}Pb_{0.2})_2Sr_2Ca_{0.25}Cu_{1.25}O_x$, $(Bi_{0.8}Pb_{0.2})_2Sr_2Ca_{0.5}Cu_{1.5}O_x$, $(Bi_{0.8}Pb_{0.2})_2Sr_2Ca_{0.75}Cu_{1.75}O_x$ and $(Bi_{0.8}Pb_{0.2})_2Sr_2Ca_{2.5}Cu_{2.5}O_x$ were simple, as follows:

$(Bi_{0.8}Pb_{0.2})_2Sr_2Ca_{0.25}Cu_{1.25}O_x$ $\xrightarrow{881^{\circ}C}$ $SrCuO_2 + L$ $\xrightarrow{950^{\circ}C}$ L
Bi(Pb)-2201+Bi(Pb)-2212

$(Bi_{0.8}Pb_{0.2})_2Sr_2Ca_{0.5}Cu_{1.5}O_x$ $\xrightarrow{881^{\circ}C}$ $(Sr,Ca)CuO_2 + L$ $\xrightarrow{960^{\circ}C}$ $(Sr,Ca)Cu_2O_3 + L$
Bi(Pb)-2201+Bi(Pb)-2212

$(Bi_{0.8}Pb_{0.2})_2Sr_2Ca_{0.75}Cu_{1.75}O_x$ $\xrightarrow{881^{\circ}C}$ $(Sr,Ca)CuO_2 + L$ $\xrightarrow{960^{\circ}C}$ $(Sr,Ca)O + L$
Bi(Pb)-2201+Bi(Pb)-2212

$(Bi_{0.8}Pb_{0.2})_2Sr_2Ca_{2.5}Cu_{2.5}O_x$ 891℃
Bi(Pb)-2212+Bi(Pb)-2223 → Amorphous+$(Sr,Ca)_2CuO_3$+L →
935℃ 960℃
→$(Sr,Ca)_2CuO_3$+(Sr,Ca)O+L →(Sr,Ca)O+L

A pseudo-binary phase diagram of the $(Bi_{0.8}Pb_{0.2})_2Sr_2CuO_6$-$CaCuO_2$ system is shown in Figure 3.19. The amorphous phase was observed above the incongruent melting point of Bi(Pb)-2223 at the $(Bi_{0.8}Pb_{0.2})_2Sr_2Ca_{2.5}Cu_{2.5}O_x$ composition. Incongruent melting points of Bi(Pb)-superconductors decrease with increasing $CaCuO_2$ besides one of the $(Bi_{0.8}Pb_{0.2})_2Sr_2Ca_{2.5}Cu_{2.5}O_x$ composition. The regions (Sr,Ca)O + L and (Sr,Ca)O + $(Sr,Ca)_2CuO_3$ + L exist in lower temperature with increasing $CaCuO_2$. Main compositions of the liquid phase were thought to be a kind of Bi-rich oxide because the composition of precipitating crystals was Sr-Ca-Cu-based oxide.

Figure 3.20 shows the phase diagrams of $(Bi_{0.8}Pb_{0.2})_2Sr_2CuO_6$-$CaCuO_2$ system reported by P. Strobel et al. which was determined using the quenching method[15]. The phase relations in the present study is roughly similar to that by P.Strobel et al. However, the detail of the phase diagram was considerably different. The main characteristics of the present phase diagram is as follows; (1) the phase diagram is simpler, (2) the clear liquidus line is determined, (3) the coexisting regions of (Sr,Ca)O and $(Sr,Ca)CuO_2$ with L appear, and (4) $(Sr,Ca)_2CuO_3$ + L region exists in a different position. The differences of present phase relation from reported ones are caused by the different experimental method, that is, in-situ observation or the analysis of quenched

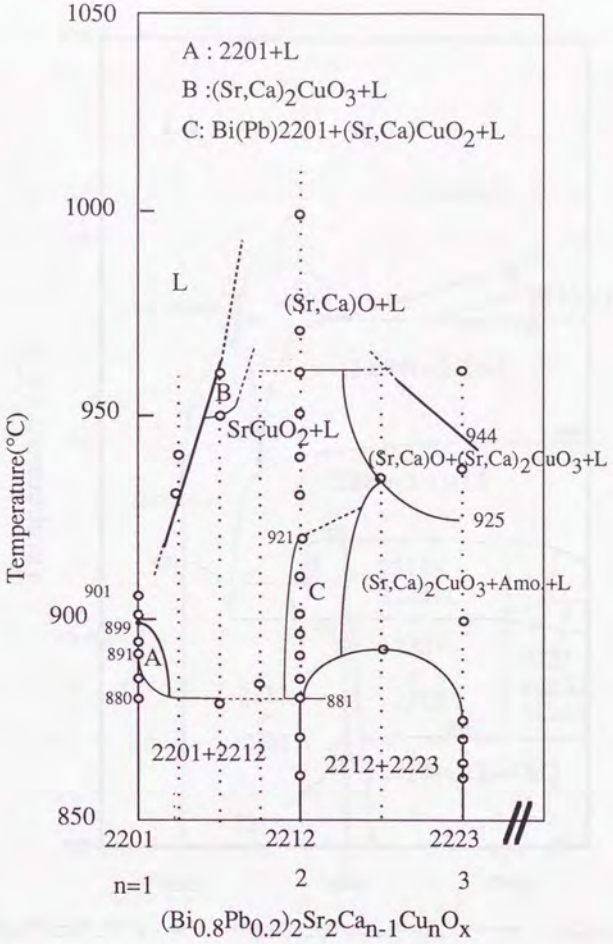

Figure 3.19 Pseudo-binary phase diagram in the $(Bi,Pb)_2Sr_2CuO_x$-$CaCuO_2$ system.

Each label means as follows,

2201:$(Bi_{0.8}Pb_{0.2})_2Sr_2CuO_6$ 2212:$(Bi_{0.8}Pb_{0.2})_2Sr_2CaCu_2O_8$

2223:$(Bi_{0.8}Pb_{0.2})_2Sr_2Ca_2Cu_3O_{10}$ Amo:Amorphous phase

Broken lines show successive mesurements on heating.

Open circles mean experimental data at fixed temperatures.

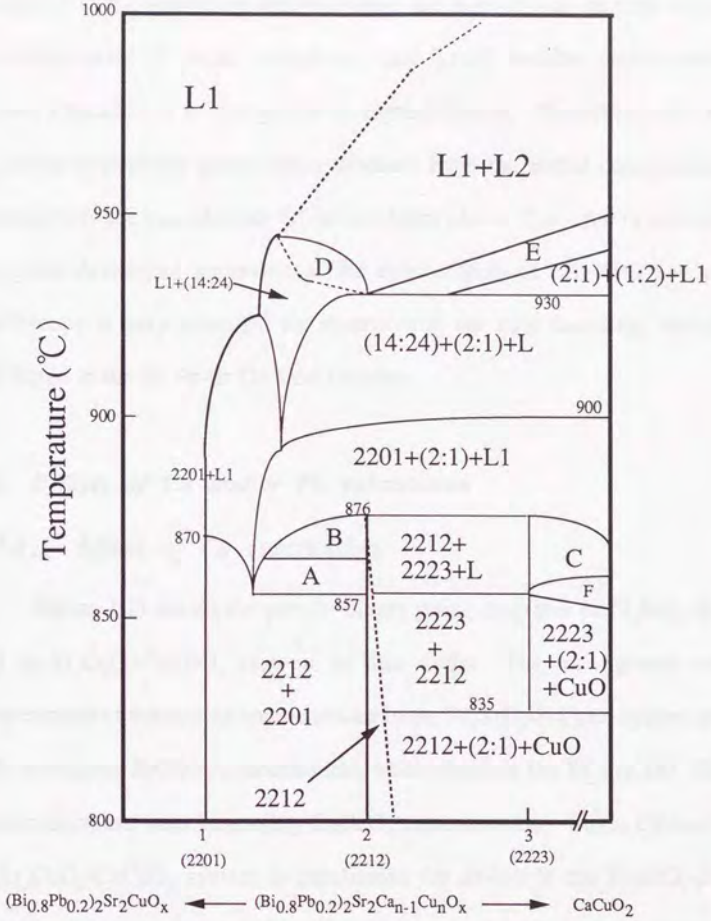

Figure 3.20 Pseudo-binary phase diagram in the $(Bi_{0.8}Pb_{0.2})_2Sr_2CuO_x$-$CaCuO_2$ system by P. Strobel et al. [15].

Each label means as follows

(2:1):$(Sr,Ca)_2CuO_3$	2212:$(Bi_{0.8}Pb_{0.2})_2Sr_2CaCu_2O_x$
(14:24):$(Sr,Ca)_{14}Cu_{24}O_x$	2223:$(Bi_{0.8}Pb_{0.2})_2Sr_2Ca2Cu_3O_x$
2201:$(Bi_{0.8}Pb_{0.2})_2Sr_2CuO_x$	
A : 2201+2212+L1+(2:1)	D : (14:24)+L1+L2
B : 2212+L1+(2:1)	E : (2:1)+(1:2)+L1+L2
C : 2223+(2:1)+L1	F ; 2223+(2:1)+CuO+L1

products. In the quenching method where the sample was quenched from the coexisting state of solid, amorphous, and liquid, another phases might be obtained because of a segregation by crystallization. Therefore, such a state including amorphous phase easily deviates from the initial composition and consequently the considerable difference takes place. Thus, the in-situ analysis using the developed apparatus of the combination of HT-XPD and optical microscopy is very powerful for determining the state including amorphous and liquid in the Bi-Pb-Sr-Ca-Cu-O system.

3.5 Effects of Ca and/or Pb substitution

3.5.1 Effect of Ca substitution

Figure 3.21 shows the pseudo-binary phase diagrams of Bi_2SrO_4-$SrCuO_2$ and $Bi_2Sr_2CuO_6$-$CaCuO_2$ systems in this study. The incongruent melting temperatures of the stoichiometric oxides in the Bi_2SrO_4-$SrCuO_2$ system increase with increasing $SrCuO_2$ concentration, while those in the $Bi_2Sr_2CuO_6$-$CaCuO_2$ system decrease with increasing $CaCuO_2$ concentration. Since Ca-ion in the $Bi_2Sr_2CuO_6$-$CaCuO_2$ system is substituted for Sr-ion in the Bi_2SrO_4-$SrCuO_2$ system, the incongruent melting temperature is thought to be determined by the Ca/Sr substitution ratio. Therefore, the opposite tendency of the incongruent melting temperature in both system is attributable to the Ca/Sr substitution. The incongruent melting temperature of Bi-2212 is about 10°C lower than that

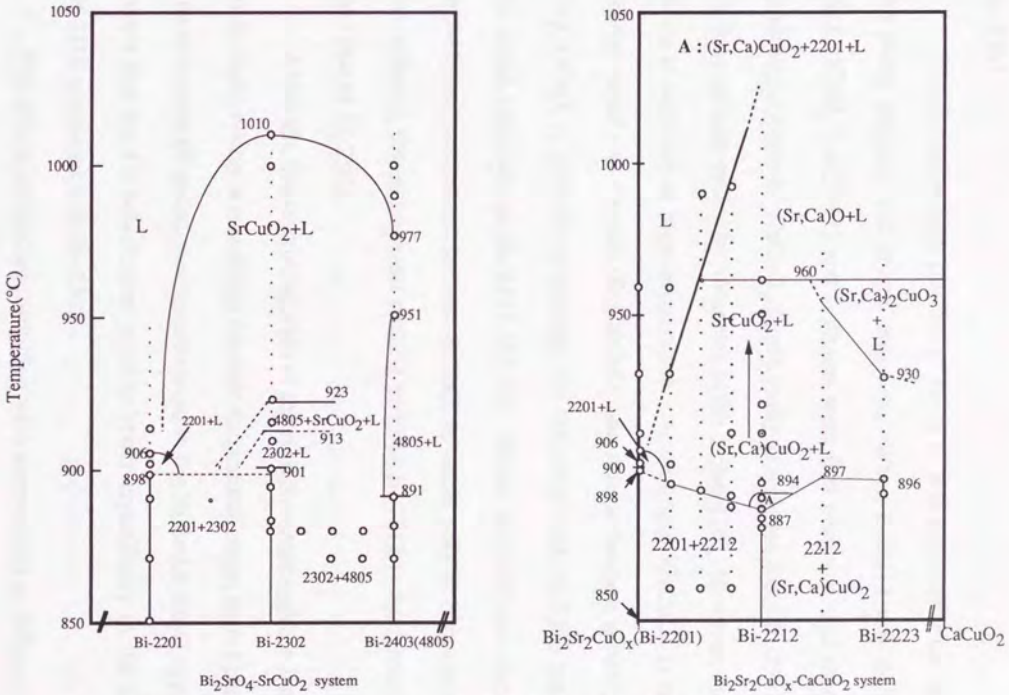

Figure 3.21 Pseudo-binary phase diagrames in the Bi_2SrO_4-$SrCuO_2$ and $Bi_2Sr_2CuO_x$-$CaCuO_2$ systems.
Broken lines show successive mesurements on heating.
Open circles mean experimental data at a fixed temperatures.
Each label means as follows;
2201:$Bi_2Sr_2CuO_6$ 2212:$Bi_2Sr_2CaCu_2O_8$ 2223:$Bi_2Sr_2Ca_2Cu_3O_{10}$
4805:$Bi_2Sr_8CuO_5$ 2302:$Bi_2Sr_3Cu_2O_x$

of Bi-2302. This means that Bi-2212 tends to decomposed more easily than Bi-2302.

The decomposition process of Bi-2212 was considered on the basis of the phase diagram and crystal structure. When Bi-2212 was decomposed, $(Sr,Ca)CuO_2$ (Ca/Sr≒1) and L phases were first observed, and then Bi-2201 gradually appeared. $CaCuO_2$ might easily precipitate from Bi-2212 because Ca-ions are surrounded by vacancies in the c-plane[16]. However, the $CaCuO_2$ phase is unstable at high-temperature. Accordingly, $CaCuO_2$ is thought to change rapidly to Ca-rich $(Sr,Ca)CuO_2$ and then to become a stable Ca-poor $(Sr,Ca)CuO_2$ (Ca/Sr≒0) on heating. On the other hand, Bi-2302 has basically the same structure as Bi-2212 [17,18]. When Bi-2302 was decomposed, $SrCuO_2$ was precipitated because $SrCuO_2$ is stable only at high-temperatures. Accordingly, the incongruent melting point of Bi-2212 is thought to be lower than that of Bi-2302.

Although, the coexisting state of the stoichiometric oxide + liquid in the Bi-Sr-Cu-O system was stable in the wide temperature range, such a phenomenon due to re-crystallization, was not observed in the Bi-Sr-Ca-Cu-O system. This means that the Ca substitution leads to better crystallinity in the powder of Bi-2212 compared with Bi-2302.

The effects of the Ca substitution were summarized as follows,

(1) The substitution changes the way of the change in the incongruent melting temperature of the stoichiometric oxides when their compositions are altered.

(2) The substitution results in the instability of the Bi-2212 crystal structure.

(3) The substitution leads to better crystallinity in and around grain boundaries in the powder with the Bi-2212 crystal structure.

3.5.2 Effect of Pb substitution

Figure 3.22 shows the pseudo-binary phase diagrams in the $Bi_2Sr_2CuO_6$-$CaCuO_2$ and $(Bi_{0.8}Pb_{0.2})_2Sr_2CuO_6$-$CaCuO_2$ systems in this study. The phase diagrams are similar to each other. Effects of the Pb substitution are as follows;

(1) The $(Sr,Ca)CuO_2$ +Bi(Pb)-2201+L phases exist in the wide temperature range between 881 and 920 °C.

(2) The incongruent melting point of Bi(Pb)-Sr-Ca based cuprates were 6~10°C lower than those of Bi-Sr-Ca based cuprate.

(3) The amount of liquid phase above the incongruent melting points of Bi(Pb)-based cuprates is larger than that of Bi-based cuprates.

(4) The amorphous phase was observed in the temperature range of about 50°C above the incongruent melting point of Bi(Pb)-2223 and $(Bi_{0.8}Pb_{0.2})_2Sr_2Ca_{2.5}Cu_{2.5}O_x$.

The difference in the incongruent melting point as listed in (2) is advantageous when synthesizing these oxides because these oxides are thought to be synthesized by so-called liquid phase sintering[19]. Actually, Bi(Pb)-based cuprates superconductors can be sintered more easily than Bi-based ones.

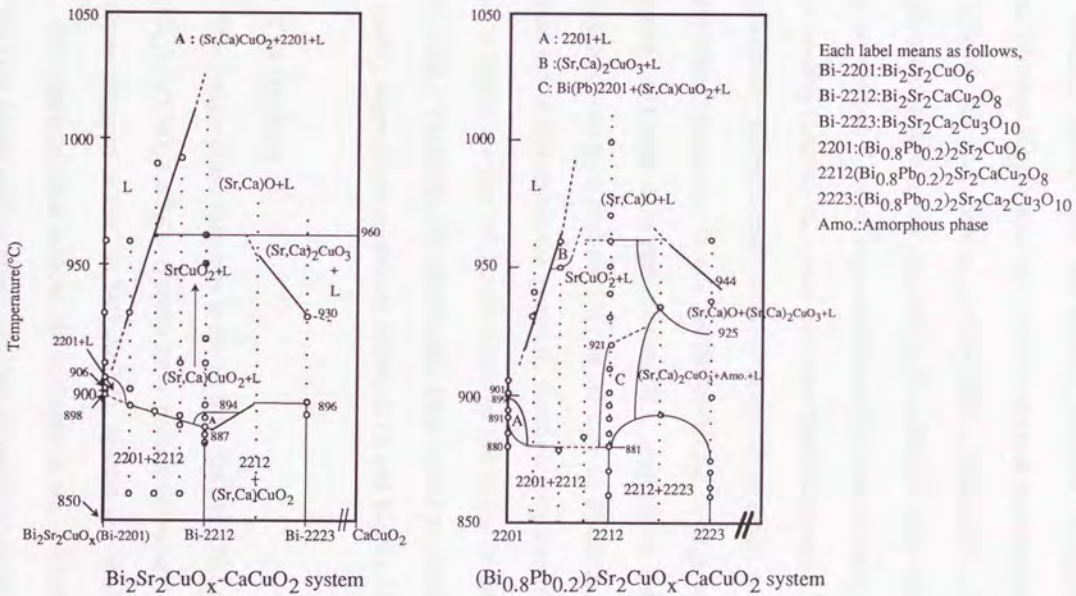

$Bi_2Sr_2CuO_x$-$CaCuO_2$ system

$(Bi_{0.8}Pb_{0.2})_2Sr_2CuO_x$-$CaCuO_2$ system

Figure 3.22 Pseudo-binary phase diagrams in the $Bi_2Sr_2CuO_x$-$CaCuO_2$ and $(Bi_{0.8}Pb_{0.2})_2Sr_2CuO_x$-$CaCuO_2$ systems.

Broken lines show successivemesurements on heating.
Open circles mean experimental data at a fixed temperature.

Bi-2212, Bi(Pb)-2212, and Bi(Pb)-2223 melt incongruently as well as Y- and Tl-based superconductors. This means that these are synthesized using the peritectic reaction, for example, Bi-2201 + $(Sr,Ca)CuO_2$ + L $\rightarrow$ Bi-2212. The peritectic reaction was reported to be useful to grow high quality large single crystals of Y-based superconductors[20] and Tl-based ones[21] using a slow cooling method from solid and melt coexisting state. Therefore, there is a possibility to grow such single crystals of Bi-based and Bi(Pb)-based cuprate superconductors. In this growth technique, a large amount of liquid coexisting solid around the peritectic reaction temperature was reported to be essential to obtain such crystals[22]. In the case of Bi-2212, a small amount of liquid exists just above the peritectic reaction temperature. On the other hand, a larger amount of liquid exists in the cases of Bi(Pb)-2212 and Bi(Pb)-2223. Therefore, Pb substitution leads to the possibility for growing high quality large single crystals of Bi(Pb)-2212 and Bi(Pb)-2223.

3.6 Conclusions

The precise phase diagrams in the Bi_2SrO_4-$SrCuO_2$, $Bi_2Sr_2CuO_6$-$CaCuO_2$, $(Bi_{0.8}Pb_{0.2})_2Sr_2CuO_6$-$CaCuO_2$ systems have been investigated in this chapter. The phase diagram in the Bi_2SrO_4-$SrCuO_2$ system is clarified for the first time. The characteristics in these phase diagrams are clarified and discussed from the view points such as phase relations, incongruent melting temperatures, liquidus line, amount of liquid and so on. The stability of the stoichiometric

oxides + Liquid is also clarified and discussed. The amorphous phases is first found to exist in the $(Bi_{0.8}Pb_{0.2})_2Sr_2CuO_6$-$CaCuO_2$ system. In addition, the effects of the Ca and/or Pb substitution on the phase diagrams are relations and discussed. The advantages of the substitution in the materials synthesis and growth are also described.

Finally, the developed apparatus in this study is found to be very powerful to decide and investigate the exact phase relations in the complicated multi-components systems where non-equilibrium phase, extremely reactive phases and/or narrow temperature regions exist.

References

[1]S.Koyama, U.Endo and T.Kawai, *Jpn. J. Appl. Phys.* **27**(1988)1861.

[2] Y.Ikeda, H.Ito, S.Shimomura, Z.Hiroi, M.Takano, Y.Bando, J.Takada, K.Oda, H.Kitaguchi, Y.Miura, Y.Takeda and T.Takada, *Physica C* **190**(1991)18.

[3] K.Shigematsu, H.Takei, I.Higashi and M.Aono, *J. Cryst. Growth*, **100**(1990)661.

[4] J.C.Soret, L.Ammor and B.Martine, *Physica C* **220**(1994)242.

[5] K.C.Hewitt, X.K.Chen, X.Meng-Burany, A.E.Curzon and J.C.Irwin, *Physica C* **251**(1995)192.

[6] Q.Y.Hu, H.K.Liu and S.X.Dou, *Physica C* **250**(1995)7.

[7] H.Maeda, Y.Tanaka, M.Fukutomi and T.Asano, *Jpn. J. Appl. Phys.* **27**(1988)209.

[8] Parity Ed. Comitt. : Parity extra volume **No.6**, High temperature superconductivity[2], (*Maruzen*,1988, Tokyo)

[9] Y.Matsui, H.Maeda, Y.Tanaka and S. Horiuch, *Jpn. J. Appl. Phys.* **27**(1988)372.

[10] N.Uno, N.Enomoto, Y.Tanaka and H.Takami, *Jpn. J. Appl. Phys.* **27** (1988) 1003.

[11] H.Komatsu, Y.Kato, S.Miyashita, T.Inoue and S. Hayashi, *Physica C*

190(1991)14.

[12] P.Strobel and T. Fournier, *J. Less-Comm. Metals*, **164&165** (1990)519.

[13] T.Hasegawa, H.Kobayashi, H.Kumakura, H.Kitaguchi, and K.Tagano, *Physica C* **222**(1994)111.

[14] S.T.Misture, D.P.Matheis, R.L.Snyder, T.N.Blanton, G.M.Zorn and B.Seebacher, *Physica C*, **250**(1995)175.

[15] P.Strobel, J.C.Toledano, D.Morin, K.Schneck. G.Vacquier, O.Monnereau, J.Primot and T.Fournier, *Physica C* **201**(1992)27.

[16] M.Onoda, A.Yamamoto, E.Takayama-Muromachi and S.Takekawa, *Jpn. J. Appl. Phys.* **27**(1988)833.

[17] S.Roth, C.Rawn, B.Burton and F.Beech; J. Res. Nat. Inst. Stand. Technol. **95**(1990)291

[18] M.A.Subramanian, A.R.Strzelecki, J. Gopalakrishnan and A.W.Sleight, *J. Solid State Chem.* **77**(1988)196.

[19] Randall M. German : Liquid Phase Sintering, (*Plenum Pub. Co.*, 1985, New York).

[20] H.Asaoka, H.Takei, Y.Iye, M.Tamura, M.Kinoshita and H.Takeya, *Jpn. J. Appl. Phys.* **32**(1993)1091.

[21] Y.Matsushita, M.Hasegawa, F.Sakai and H.Takei, *Jpn. J. Appl. Phys.*

34(1995)1263.

[22] H.Asaoka, H.Takei and K.Noda, *Jpn. J. Appl. Phys.* **33**(1994)923.

Chapter 4. Conclusions

(I) The high temperature X-ray powder diffraction apparatus with PSPC combined with the optical microscope has been developed. The optimum operation conditions of the developed apparatus have been established. The capabilities of the apparatus are as follows;

(1) The highest temperature of the sample can be set at 1100 °C and the sample temperature can be controlled at a rate between 1 to 20°C/min by a computer.

(2) The sample chamber can be evacuated or filled with air, oxygen, or inert gas.

(3) The sample holder can be set in a horizontal position to measure a coexisting state of solid and melt. It is possible to apply a rotation around the vertical axis to eliminate a preferred of crystal orientations.

(4) The total accumulation time of scattered X-rays ($\Delta 2\theta$=40°) is less than 1 min.

(5) The view of sample surface can be observed with the magnification about 100 times on the TV monitor.

(6) The sample can be kept at the right position during measurement by the microscope focus adjustment.

(II) The precise phase diagrams in the Bi_2SrO_4-$SrCuO_2$, $Bi_2Sr_2CuO_6$-$CaCuO_2$, $(Bi_{0.8}Pb_{0.2})_2Sr_2CuO_6$-$CaCuO_2$ system have been clarified for the first time. The stable coexisting region of the stoichiometric oxides + liquid was discovered in the Bi-Sr-Cu-O system, accompanying with a complicated change of the liquid amount. The amorphous phase coexisting with crystal solid and liquid was discovered above the incongruent melting points in the Bi(Pb)-2223 and $(Bi_{0.8}Pb_{0.2})_2Sr_2Ca_{2.5}Cu_{2.5}O_x$ in the $(Bi_{0.8}Pb_{0.2})_2Sr_2CuO_6$-$CaCuO_2$ systems. The effects of Ca and/or Pb substitution on the phase relations are summarized as follows;

The Ca substitution;

(1) The substitution has a remarkable effect for changing in the incongruent melting temperature of the stoichiometric oxides with an alternation of their compositions changes.

(2) The substitution results in the instability of the Bi-2212 crystal structure.

(3) The substitution leads to better crystallinity in and around grain boundaries in the powder with the Bi-2212 crystal structure.

The Pb substitution;

(1) The substitution leads to the region of $(Sr,Ca)CuO_2$ +Bi(Pb)-2201+L

in the wide temperature range between 881 and 920 °C.

(2) The effects of substitution results of Bi for Pb in the 6~10°C decrease of the incongruent melting point of Bi(Pb)-Sr-Ca based cuprates compared with that of Bi-Sr-Ca based cuprate.

(3) The above substitution also results in the increase of the amount of liquid above the incongruent melting points of Bi(Pb)-Sr-Ca based cuprates compared with those of Bi-Sr-Ca based cuprates.

(4) The same substitution as above leads to the occurrence of the amorphous phase in the temperature range of about 50°C above the incongruent melting point of Bi(Pb)-2223 and $(Bi_{0.8}Pb_{0.2})_2Sr_2Ca_{2.5}Cu_{2.5}O_x$.

Acknowledgments

The author wishes to express his greatest appreciation to Professor Humihiko Takei of Institute for Solid State Physics (ISSP), the University of Tokyo, for his many positive advice and support, heartful encouragement and lucid guidances on the research. Hearty thanks are also given to Professor Masamichi Miyamoto of Mineralogical Institute, Faculty of Science, The University of Tokyo, for his encouragement and support. He also express his gratitude to Professors Hiroyuki Horiuchi, Tokuhei Tagai and Tohru Ozawa of Mineralogical Institute, Faculty of Science, The University of Tokyo, for their enthusiastic advice and suggestions. He gratefully acknowledges to Dr. Masashi Hasegawa of ISSP for his warm encouragement and many useful discussions. He expresses appreciation to Ms. Fumiko Sakai of ISSP for her many advice and guidances on chemical analysis. He gratefully acknowledges to Dr. Yasunao Oyama of Faculty of Science, University of Gakushuin, and Mr. Masayoshi Koike of ISSP for their advice and supports on experimental techniques. He is also grateful very much to Mr. Ken-ichi Yumoto and Mr. Mikito Mamiya for their kind help of experiments and analytical researches for a long time. He thanks Mr. Zyao Tang-long, Mr. Masayuki Tanaka and Mr. Yan Zheng for their useful discussions and warm advice. Finally, the author express his best acknowledgments to his parents and sisters for

their financial and spiritual supports through nine years of university and graduate students life.

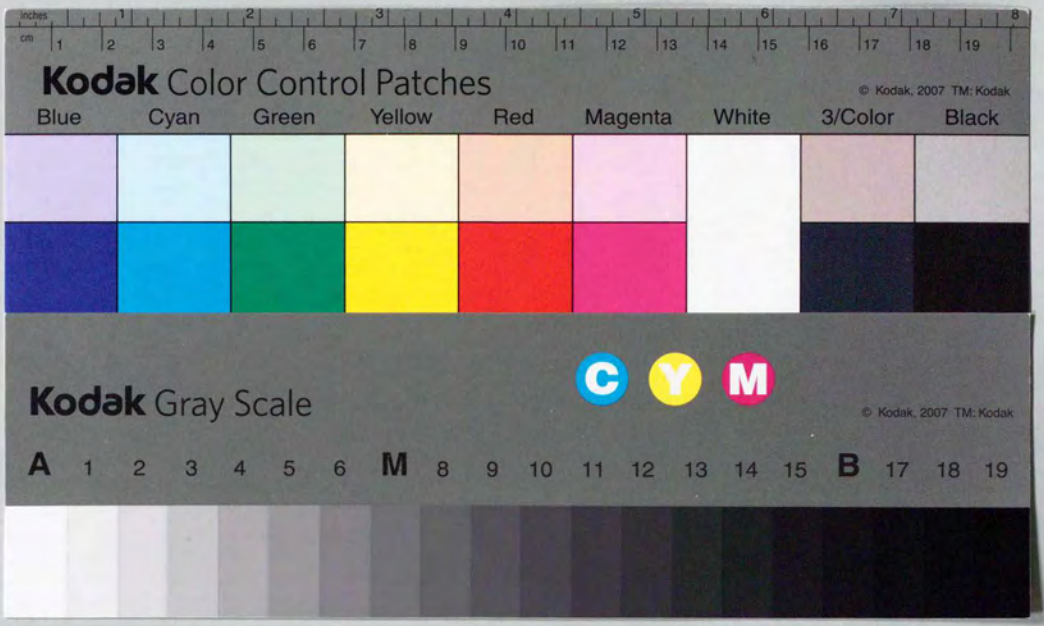
inches
cm
Kodak Color Control Patches
© Kodak, 2007 TM: Kodak
Blue
Cyan
Green
Yellow
Red
Magenta
White
3/Color
Black
Kodak Gray Scale
C
Y
M
© Kodak, 2007 TM: Kodak
A 1 2 3 4 5 6 M 8 9 10 11 12 13 14 15 B 17 18 19